However, the combined assay with α4GnT mRNA can detect pancreatic cancer patients more efficiently when compared with the enzyme immunoassays targeting single biomarkers.

The present study also demonstrated that the expression levels of α4GnT mRNA were elevated in 40% of chronic pancreatitis patients and 17% of cancer-free volunteers, albeit at much lower levels than those of pancreatic cancer patients. Previously, we showed that significant amounts α4GnT mRNA were detected in patients with *H. pylori* infection or chronic gastroduodenal ulcers.[17] It has been reported that unexpected genes such as α-fetoprotein are transcribed in lymphocytes when they are activated,[25] suggesting the possibility that α4GnT mRNA might be induced in the activated lymphocytes circulating in the *H. pylori*-infected patients. However, as shown previously[17] and further confirmed here, we have demonstrated that α4GnT mRNA is not detectable in activated lymphocytes or resting lymphocytes. By contrast, we have also reported that extensive biopsy of the gastric mucosa results in elevation of the α4GnT mRNA level in peripheral blood.[26] These results combined suggest that the gastric gland mucous cells expressing α4GnT mRNA enter the bloodstream through the injured sites of gastric mucosa caused by inflammation or biopsy. Considering the high incidence of *H. pylori* infection in individuals over 40 years of age in Japan,[27,28] α4GnT mRNA detected in the cancer-free volunteers is most likely derived from gastric gland mucous cells that have entered the peripheral blood through injured sites of the gastric mucosa caused by *H. pylori* infection. We previously demonstrated that α4GnT mRNA is not detected in the peripheral blood of healthy volunteers without *H. pylori* infection.[17] Similary, it may also be possible that α4GnT mRNA detected in the chronic pancreatitis patients originated from the α4GnT-positive pancreatic duct epithelia entering the blood circulation, because the disruption of pancreatic ducts could occur in chronic pancreatitis (Fig. 1c).[29] Further studies will be of significance to identify the cells that elevate the α4GnT mRNA level in the peripheral blood of these non-cancerous patients.

Recently we demonstrated that α4GnT is expressed not only in pancreatic carcinoma cells but also in biliary tract carcinoma cells that produce α1,4-GlcNAc-capped *O*-glycans.[15] Thus, the α4GnT assay will also be applicable to the detection of patients with biliary tract cancers. We have shown that α4GnT mRNA was detected in three of five patients with biliary tract cancer.[17] It is of great significance to determine the clinical utility of the α4GnT assay for diagnosis of biliary tract cancer as well.

Collectively, our results obtained in the present study indicate that quantitative analysis of α4GnT mRNA expressed in the peripheral blood allowed us to detect pancreatic cancer cells expressing α1,4-GlcNAc-capped *O*-glycans. In order to clarify the clinical contribution of this assay system, prospective controlled trials are needed in the screening, diagnosis and monitoring of pancreatic cancer patients.

Acknowledgments

This study was supported by Grant-in-Aids for 3rd Term Comprehensive Control Research for Cancer from the Ministry of Health, Labor and Welfare of Japan and Scientific Research on Priority Areas 14030032 and 14082201 from the Ministry of Education, Culture, Sports, Science and Technology of Japan (to JN), and by NIH Grant CA48737 from the National Institutes of Health (to MF). The authors thank Drs Tsutomu Katsuyama and Fukuto Maruta for encouragement during this work. We are also grateful to Dr Elise Lamar for critical reading of the manuscript.

References

1 Warshaw AL, Castillo CF. Pancreatic carcinoma. *N Engl J Med* 1992; **326**: 455–65.
2 Wagner M, Redaelli C, Lietz M *et al.* Curative resection is the single most important factor determining outcome in patients with pancreatic adenocarcinoma. *Br J Surg* 2004; **91**: 586–94.
3 Kuroki T, Tomioka T, Tajima Y *et al.* Detection of the pancreas-specific gene in the peripheral blood of patients with pancreatic carcinoma. *Br J Cancer* 1999; **81**: 350–3.
4 Iacobuzio-Donahue CA, Maitra A, Shen-Ong GL *et al.* Discovery of novel tumor markers of pancreatic cancer using global gene expression technology. *Am J Pathol* 2002; **160**: 1239–49.
5 Gold P, Freedman S. Demonstration of tumor-specific antigens in human colonic carcinoma by immunological tolerance and absorption techniques. *J Exp Med* 1965; **121**: 439–62.
6 Koprowski H, Steplewski Z, Mitchell K, Herlyn M, Herlyn D, Fuhrer P. Colorectal carcinoma antigens detected by hybridoma antibodies. *Somatic Cell Genet* 1979; **5**: 957–72.
7 Metzgar RS, Rodriguez N, Finn OJ *et al.* Detection of a pancreatic cancer-associated antigen (DU-PAN-2 antigen) in serum and ascites of patients with adenocarcinoma. *Proc Natl Acad Sci USA* 1984; **81**: 5242–6.
8 Haviland AE, Borowitz MJ, Killenberg PG, Lan MS, Metzgar RS. Detection of an oncofetal antigen (DU-PAN-2) in sera of patients with non-malignant hepatobiliary disease and hepatomas. *Int J Cancer* 1988; **41**: 789–93.
9 Kiriyama S, Hayakawa T, Kondo T *et al.* Usefulness of a new tumor marker, span-1, for the diagnosis of pancreatic cancer. *Cancer* 1990; **65**: 1557–61.
10 Koopmann J, Zhang Z, White N *et al.* Serum diagnosis of pancreatic adenocarcinoma using surface-enhanced laser desorption and ionization mass spectrometry. *Clin Cancer Res* 2004; **10**: 860–8.
11 Rosewicz S, Wiedenmann B. Pancreatic carcinoma. *Lancet* 1997; **349**: 485–9.
12 Nakamura N, Ota H, Katsuyama T *et al.* Histochemical reactivity of normal, metaplastic, and neoplastic tissues to α-linked *N*-acetylglucosamine residue-specific monoclonal antibody HIK1083. *J Histochem Cytochem* 1998; **46**: 793–801.
13 Hruban RH, Goggins M, Parsons J, Kern SE. Progression model for pancreatic cancer. *Clin Cancer Res* 2000; **6**: 1835–9.
14 Nakayama J, Yeh J-C, Misra AK, Ito S, Katsuyama T, Fukuda M. Expression cloning of a human α1,4-*N*-acetylglucosaminyltransferase that forms GlcNAcα1→4Galβ→R, a glycan specifically expressed in the gastric gland mucous cell-type mucin. *Proc Natl Acad Sci USA* 1999; **96**: 8991–6.
15 Nakajima K, Ota H, Zhang MX *et al.* Expression of gastric gland mucous cell-type mucin in normal and neoplastic human tissues. *J Histochem Cytochem* 2003; **51**: 1689–98.
16 Zhang MX, Nakayama J, Hidaka E *et al.* Immunohistochemical demonstration of α1,4-N-acetylglucosaminyltransferase that forms GlcNAcα1,4Galβ residues in human gastrointestinal mucosa. *J Histochem Cytochem* 2001; **49**: 587–96.
17 Shimizu F, Nakayama J, Ishizone S *et al.* Usefulness of the real-time reverse transcription–polymerase chain reaction assay targeted to α1,4-*N*-acetylglucosaminyltransferase for the detection of gastric cancer. *Lab Invest* 2003; **83**: 187–97.
18 Sobin LH, Wittekind C, eds. *TNM Classification of Malignant Tumours*, 5th edn. New York, NY: John Wiley-Liss, 1997.
19 Machida E, Nakayama J, Amano J, Fukuda M. Clinicopathological

significance of core2 β1,6-*N*-acetylglucosaminyltransferase messenger RNA expressed in the pulmonary adenocarcinoma determined by *in situ* hybridization. *Cancer Res* 2001; **61**: 2226–31.
20 Kawakubo M, Ito Y, Okimura Y *et al.* Natural antibiotic function of a human gastric mucin against *Helicobacter pylori* infection. *Science* 2004; **305**: 1003–6.
21 Ziske C, Schlie C, Gorschluter M *et al.* Prognostic value of CA19-9 levels in patients with inoperable adenocarcinoma of the pancreas treated with gemcitabine. *Br J Cancer* 2003; **89**: 1413–17.
22 Tanaka N, Okada S, Ueno H, Okusaka T, Ikeda M. The usefulness of serial changes in serum CA19-9 levels in the diagnosis of pancreatic cancer. *Pancreas* 2000; **20**: 378–81.
23 Koopmann J, Buckhaults P, Brown DA *et al.* Serum macrophage inhibitory cytokine 1 as a marker of pancreatic and other periampullary cancers. *Clin Cancer Res* 2004; **10**: 2386–92.
24 Nakao A, Oshima K, Nomoto S *et al.* Clinical usefulness of CA19-9 in pancreatic carcinoma. *Semin Surg Oncol* 1998; **15**: 15–22.
25 Lafarge-Frayssinet C, Torres JM, Frain M, Uriel J. α-Fetoprotein gene expression in human lymphoblastoid cells and in PHA-stimulated normal T-lymphocytes. *Biochem Biophys Res Commun* 1989; **159**: 112–18.
26 Shimizu F, Nakayama J, Sugiyama A, Kawasaki S, Katsuyama T. Gastric gland mucous cells circulate in peripheral blood after endoscopic biopsy of the gastric mucosa. *Am J Gastroenterol* 2000; **95**: 3017–18.
27 Asaka M, Kimura T, Kudo M *et al.* Relationship of *Helicobacter pylori* to serum pepsinogens in an asymptomatic Japanese population. *Gastroenterology* 1992; **102**: 760–6.
28 Matsuhisa TM, Yamada NY, Kato SK, Matsukura NM. *Helicobacter pylori* infection, mucosal atrophy and intestinal metaplasia in Asian populations: A comparative study in age-, gender- and endoscopic diagnosis-matched subjects. *Helicobactor* 2003; **8**: 29–35.
29 Oertel JE, Oertel YC, Heffess CS. Pancreas. In: Sternberg SS, ed. *Diagnositic Surgical Pathology*. New York: Raven Press, 1994; 1419–57.

doi: 10.1111/j.1349-7006.2006.00148.x

THE JOURNAL OF BIOLOGICAL CHEMISTRY
Vol. 279, No. 4, Issue of January 23, pp. 3058–3067, 2004
Printed in U.S.A.

Core 2 Branching β1,6-*N*-Acetylglucosaminyltransferase and High Endothelial Venule-restricted Sulfotransferase Collaboratively Control Lymphocyte Homing*

Received for publication, October 10, 2003, and in revised form, October 28, 2003
Published, JBC Papers in Press, October 30, 2003, DOI 10.1074/jbc.M311150200

Nobuyoshi Hiraoka‡§, Hiroto Kawashima‡§, Bronislawa Petryniak¶, Jun Nakayama‖, Junya Mitoma‡, Jamey D. Marth, John B. Lowe¶, and Minoru Fukuda‡ ‡‡**

*From the ‡Glycobiology Program, Cancer Research Center, The Burnham Institute, La Jolla, California 92037, the ¶Howard Hughes Medical Institute, Department of Pathology, The University of Michigan Medical School, Ann Arbor, Michigan 48109, the ‖Department of Pathology, Shinshu University School of Medicine, Matsumoto 390-8621, Japan, and the **Howard Hughes Medical Institute, Division of Cellular and Molecular Medicine, University of California, San Diego, La Jolla, California 92093*

L-selectin mediates lymphocyte homing by facilitating lymphocyte adhesion to carbohydrate ligands expressed on high endothelial venules (HEV) of the secondary lymphoid organs. Previous studies demonstrated that L-selectin ligand sulfotransferase (LSST) forms 6-sulfo sialyl Lewis x (sLe^x) on both core 2 branch and MECA-79-positive extended core 1 *O*-glycans, but the chemical nature and roles of HEV ligands elaborated by LSST and core 2 β1,6-*N*-acetylglucosaminyltransferase-1 (Core2GlcNAcT) have been undefined. In the present study, we have generated mutant mice with deficient LSST and show that inactivation of LSST gene alone leads to only partial impairment of lymphocyte homing to peripheral lymph nodes and moderate reduction in lymphocyte counts in the peripheral lymph nodes, despite the fact that L-selectin ligands that contain 6-sulfo sLe^x are reduced at HEV. By contrast, LSST/Core2GlcNAcT double null mice exhibited a markedly reduced lymphocyte homing and reduced lymphocyte counts as a result of significantly decreased 6-sulfo sLe^x on HEV L-selectin counterreceptors, relative to LSST- or Core2GlcNAcT-single null mice. Moreover, induction of LSST and Core2GlcNAcT transcripts was observed in HEV-like structure formed in the salivary gland of the non-obese diabetic mouse, which displays chronic inflammation. These results indicate that LSST and Core2GlcNAcT cooperatively synthesize HEV-specific L-selectin ligands required for lymphocyte homing and suggest that LSST and Core2GlcNAcT play a critical role in lymphocyte trafficking during chronic inflammation.

Lymphocyte recirculation through lymph nodes and Peyer's patches is important for detection of foreign antigens by the immune system and subsequent processes that neutralize these molecules. Lymphocyte recirculation critically depends on interaction between the leukocyte adhesion molecule L-selectin and counterreceptors restricted on specialized post capillary venules, high endothelial venules (HEV)[1] in secondary lymphoid organs. The counterreceptors on the luminal surface of HEV capture circulating lymphocytes via L-selectin-dependent adhesive interactions that lead, in turn, to lymphocyte tethering and rolling, chemokine-dependent activation, integrin-mediated firm attachment, and lymphocyte transmigration (1–4). L-selectin and its ligands are also implicated in lymphocyte recruitment in certain chronic inflammation. HEV-like microvasculature is induced on endothelium in association with insulitis characteristic of the non-obese diabetic (NOD) mouse and the rejection of heart transplants in rodents and humans (5–8). Similarly, HEV-like structure is observed in inflammatory bowel diseases, rheumatoid arthritis, lymphocytic thyroiditis, and the hyperplastic thymus of the AKR mouse (9–12). It has been suggested that recruitment of lymphocytes by induced L-selectin ligand may contribute to the pathogenesis of these diseases, which is characteristic of induced HEV-like microvasculature.

L-selectin present on leukocytes is a carbohydrate-binding protein characterized by dependence on Ca^{2+} for its activity. HEV-borne L-selectin counterreceptors include GlyCAM-1, CD34, podocalyxin, Sgp200, endoglycan, and MAdCAM-1, all of which have mucin-like domains that act as scaffolding for *O*-linked oligosaccharides (13). The function of these L-selectin counterreceptors entirely depends on their decoration with specific sialylated, fucosylated, and sulfated oligosaccharides, which contain 6-sulfo sialyl Lewis X (sLe^x), (NeuNAcα2→3Galβ1→4[Fucα1→3(sulfo→6)]GlcNAcβ1→R) (14–17). Indeed, recent studies demonstrate that mouse and human L-selectin ligand sulfotransferase (LSST, also known as HEC-GlcNAc6ST or GlcNAc6ST-2 (18)) is capable of forming 6-sulfo sLe^x on core 2-branched *O*-glycans (16, 19). More recent studies demonstrated that LSST together with core 1 extension enzyme (Core1-β3GlcNAcT) forms the MECA-79 epitope, defined as Galβ1→4(sulfo→6)GlcNAcβ1→3Galβ1→3GalNAcα1→R, which is a partial structure of 6-sulfo sLe^x on extended core 1 *O*-glycans (20). The MECA-79 antibody also binds to 6-sulfo sLe^x on extended core 1 and inhibits both *in*

* The work was supported by Grants PO1CA71932 (to M. F. and J. B. L.), DK48247 (to J. D. M.), and R37CA33000 (to M. F.) from the National Institutes of Health, by Howard Hughes Investigator Awards (to J. B. L. and J. D. M.), and by Priority Area 14082201 (to J. N.) from the Ministry of Education, Culture, Sports, Science and Technology of Japan. The costs of publication of this article were defrayed in part by the payment of page charges. This article must therefore be hereby marked "*advertisement*" in accordance with 18 U.S.C. Section 1734 solely to indicate this fact.

§ Both authors equally contributed to the work.

‡‡ To whom correspondence should be addressed: The Burnham Institute, 10901 North Torrey Pines Rd., La Jolla, CA 92037. Tel.: 858-646-3144; Fax: 858-646-3193; E-mail: minoru@burnham.org.

[1] The abbreviations used are: HEV, high endothelial venule; LSST, L-selectin ligand sulfotransferase; Core2GlcNAcT, β1,6-*N*-acetylglucosaminyltransferase-1; Core1-β3GlcNAcT, core 1 extension β1,3-*N*-acetylglucosaminyltransferase; sLe^x, sialyl Lewis x; NOD, non-obese diabetic; EGFP; enhanced green fluorescent protein; CMFDA, 5-chloromethyl fluorescence diacetate; GlcNAc6ST-1, GlcNAc-6-*O*-sulfotransferase-1; HPLC, high performance liquid chromatography; ES cells, embryonic stem cells.

vivo and *ex vivo* lymphocyte attachment to HEV by neutralizing L-selectin ligands (20, 21). Significantly, 6-sulfo sLe^x on either extended core 1 (20)- or core 2-branched *O*-glycans provides greater L-selectin-dependent cell adhesion under shear force than does 6-sulfo sLe^x on *N*-glycans (16, 20, 22). Moreover, 6-sulfo sLe^x on bi-antennary *O*-glycans containing both core 2 branch and core 1 extension yield more efficient L-selectin-dependent cell adhesion than 6-sulfo sLe^x on core 2 branch or core 1 extension alone, indicating a synergistic effect of bivalent ligands on L-selectin-mediated adhesion (20).

Gene inactivation of LSST through homologous recombination results in significant reduction in lymphocyte homing and loss of MECA-79 at the luminal side of HEV. LSST null (LSST$^\Delta$) mice, however, still exhibit slightly over 50% of lymphocyte homing to the peripheral lymph nodes relative to wild-type mice (23; our results shown below). These observations thus indicate that 6-sulfo sLe^x on extended core 1 *O*-glycans is almost absent in LSST null mice, but 6-sulfo sLe^x on other structures remaining after inactivation of LSST must play a role as L-selectin ligands. One of those ligands is likely to be 6-sulfo sLe^x on core 2-branched *O*-glycans (16, 20). The formation of 6-sulfo sLe^x on core 2-branched *O*-glycans requires core 2 β1,6-*N*-acetylglucosaminyltransferase-I (Core2GlcNAcT) (24). In Core2GlcNAcT null (Core2GlcNAcT$^\Delta$) mice established previously, L-, P-, or E-selectin ligand on neutrophils was significantly diminished. Concomitantly, neutrophil recruitment to inflamed peritoneum in Core2GlcNAcT$^\Delta$ mice was diminished to 20% of levels seen in wild-type mice (25). However, the same studies showed that Core2GlcNAcT$^\Delta$ mice exhibited only partial reduction in lymphocyte homing and lymphocyte counts in the peripheral lymph nodes. Analysis of *O*-glycans remaining after Core2GlcNAcT inactivation demonstrated that no core 2-branched *O*-glycans was detected in GlyCAM-1 isolated from HEV and that the majority of *O*-glycans contains core 1 extension in HEV of Core2GlcNAcT$^\Delta$ mice (20). These results suggest that almost all of the 6-sulfo sLe^x on L-selectin counterreceptors reside either on core 2-branch or extended core 1 *O*-glycans. However, precise structures of these *O*-glycans and their roles in lymphocyte homing have remained undefined.

To determine the roles of LSST and Core2GlcNAcT in L-selectin ligand biosynthesis at HEV, we first generated mutant mice deficient in LSST and then generated double knockout mice deficient in both LSST and Core2GlcNAcT by cross-breeding LSST$^\Delta$ mice with Core2GlcNAcT$^\Delta$ mice, which had been previously established (25). Double knockout mice deficient in both LSST and Core2GlcNAcT exhibited significantly reduced lymphocyte homing activity and lymphocyte numbers in the peripheral lymph nodes, compared with single knockout LSST$^\Delta$ or Core2GlcNAcT$^\Delta$ mice, or to wild-type mice. In addition, LSST and Core2GlcNAcT transcripts were detected in HEV-like microvaculate endothelium formed in the salivary gland of NOD mice. These results together with structural analysis of HEV-derived *O*-glycan ligands demonstrate that LSST and Core2GlcNAcT cooperatively synthesize L-selectin ligands and together play dominant roles in lymphocyte homing and suggest that LSST and Core2GlcNAcT play a critical role in lymphocyte trafficking during chronic inflammation.

EXPERIMENTAL PROCEDURES

Generation of Targeted ES Cells—A genomic fragment of ~25 kb containing mouse LSST gene was isolated from a mouse genomic library as a BAC clone (Research Genetics) and subcloned into pBluescript II SK(−) (Stratagene). To disrupt the enzymatic function of mouse LSST, and to create a fusion protein of enhanced green fluorescent protein (EGFP) with the N terminus of LSST, including the short cytoplasmic domain, transmembrane domain, and stem region, a 1-kb NdeI and BglII segment of the LSST gene encoding the catalytic domain was replaced with a 2-kb fragment carrying EGFP-F and the G418 resistance selection (PGKneo) cassette. The inserted EGFP-F segment containing EGFP coding sequences plus the Ras farnesylation signal, and an SV40 poly(A) signal was prepared by amplification of pEGFP-F vector (Clontech), in which the multicloning sites had been deleted by PCR using 5′-TCCATATGTCCGTCCACAGACACCTTATGGTGAGCA-AGGGCGAGGAG-3′ (5′-primer) and 5′-CGGGATCCGCGTTAAGATA-CATTGATGAGTTTG-3′ (3′-primer). The EGFP-F and PGKneo cassette was flanked by 1 kb of mouse genomic DNA at its 5′ region and by 4.5 kb of mouse genomic DNA at its 3′ region. The targeting vector was linearized and electroporated into R1 ES cells. ES cells were positively selected for G418 resistance and negatively selected by expression of the diphtheria toxin gene, inserted into the targeting vector. Targeting events were identified by PCR amplification with EGFP-specific primer (R1M) and a primer (F1M) specific for a LSST sequence outside the LSST sequence contained in the targeting vector (see Fig. 1*A*). ES cells positively screened by PCR were confirmed by Southern blot analysis using XbaI digestion and the genomic probe A in the 5′ region of homologous recombination (20 kb WT, 10.5 kb mutant) and EcoRV digestion and genomic probe B in the 3′ arm of the LSST genome using the targeting vector (30 kb WT, 5 kb mutant).

Generation of LSSTΔ Mice and LSST$^\Delta$/Core2GlcNAcT$^\Delta$ Mice—Chimeric males were produced by injection of LSST$^{+/-}$ ES cells into blastocysts and were bred with C57BL/6 females to produce F1 heterozygotes. Germ line transmission was confirmed by PCR, and LSST$^{+/-}$ progeny were backcrossed onto C57BL/6 wild-type mice. Heterozygous males and females were mated to produce wild-type, heterozygous, and homozygous mutant animals. For PCR analysis to genotype the mice, genomic DNA was purified from mouse tail and used as template. F1M and R1M primer pairs were used for detection of the mutated allele. For detection of the wild-type allele, F1W and R1W were used (see Fig. 1*A*). In some analyses, the following PCR primers were used for simultaneous detection of wild-type and mutant alleles in the same PCR reaction; 5′-AAGAAAGGGAGGCTGCTGATGTTC-3′ (F2W) was used as the 5′-primer and 5′-TCCACCATATCAAAGGGCTGCTGA-3′ (R2W) and R1M as 3′-primers. LSST$^\Delta$ mice were back-crossed with C57BL/6 for a total of three generations. C57BL/6 Core2GlcNAcT$^\Delta$ mice and C57BL/6 LSST$^\Delta$ mice were then bred to generate a C57BL/6 LSST$^\Delta$/Core2GlcNAcT$^\Delta$ strain.

Detection of LSST-GFP Chimeric Protein and MECA-79 Antigen and Binding of L-selectin-IgM Chimeric Protein to HEV—The extracellular domain of human L-selectin was amplified by PCR and linked to the DNA sequence encoding for the CH2, CH3, and CH4 domains of human IgM in pcDNA1.1 as described for the mouse L-selectin IgM chimera (26). Binding of L-selectin-IgM was detected by goat biotinylated anti-human IgM antibodies followed by Texas red-conjugated avidin. MECA-79 antigen was detected using MECA-79 antibody (BD Pharmingen (21)), followed by rhodamine-conjugated goat anti-rat IgM. The expression of LSST in HEV was detected by fluorescence derived from LSST-EGFP chimeric protein.

Isolation of GlyCAM-1—GlyCAM-1 was prepared from sera of wild-type and LSST$^\Delta$ mice as described previously (27). The samples were subjected to SDS-PAGE, blotted to a nitrocellulose membrane and reacted with anti-GlyCAM-1 antibodies that had been prepared as described previously (27), or MECA-79 antibody followed by goat anti-rabbit immunoglobulins and goat anti-rat IgM antibodies, respectively. The bound antibodies were visualized by ECL (Amersham Biosciences).

Structural Analysis of Oligosaccharides Attached to GlyCAM-1—Axillary, cervical, and mesenteric lymph nodes from wild-type, LSST$^\Delta$, Core2GlcNAcT$^\Delta$, or LSST$^\Delta$/Core2GlcNAcT$^\Delta$ mice were metabolically labeled with 0.5 mCi/ml [^{3}H]galactose (20). GlyCAM-1 was purified from the condition medium using a column of anti-GlyCAM-1 antibodies conjugated to UltraLink Biosupport Medium (Pierce), as described previously (27).

O-Glycans from the purified GlyCAM-1 were isolated and separated by QAE-Sephadex A-25 column chromatography in 10 mM pyridine-acetate buffer (pH 5.5) before and after removal of sialic acid by mild acid hydrolysis as described previously (20, 28). Monosulfated, disulfated, and trisulfated *O*-glycans, eluted with 70 mM, 120 mM (plus 140 mM), and 250 mM (plus 300 mM) NaCl, respectively, were separately applied to a Bio-Gel P-4 gel filtration column as described previously (16, 20).

Fractionated *O*-glycans were then sequentially treated with α1,3-fucosidase and Jack bean β-galactosidase followed by β-*N*-acetylhexosaminidase B, which cleaves only non-sulfated *N*-acetylglucosamine. After these digestions, the majority of oligosaccharides should yield (sulfo→6)GlcNAcβ1→6(Galβ1→3)GalNAcOH from sulfated core 2-branch *O*-glycans and (sulfo→6)GlcNAcβ1→3Galβ1→3GalNAcOH from sulfated, extended core 1 *O*-glycans, respectively. These two com-

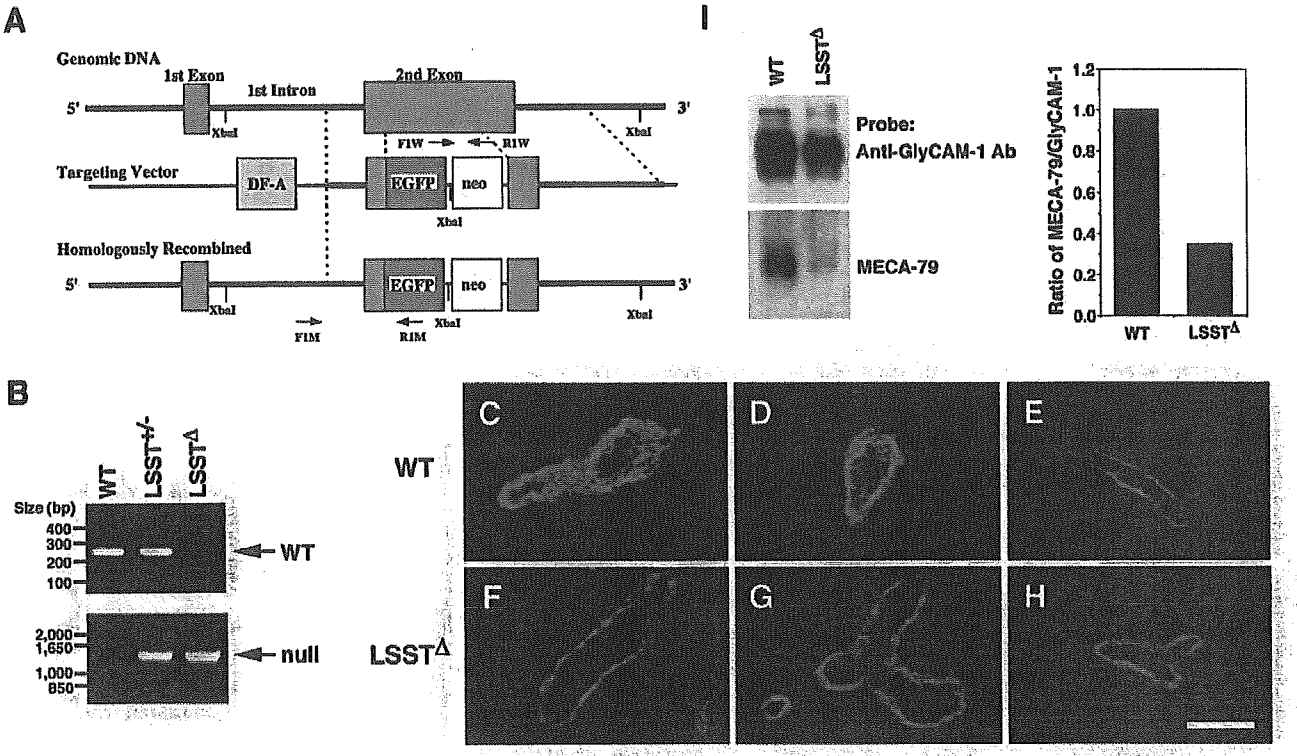

FIG. 1. **Inactivation of the LSST locus.** *A*, structure of wild-type and mutant LSST Loci. The targeting vector replaces the DNA encoding amino acid residues (33–388) of LSST with cDNA encoding EGFP and the herpes virus thymidine kinase cassette (Neo). The targeted allele encodes the cytoplasmic, transmembrane, and stem regions of LSST fused with EGFP under control of the LSST promoter. Diphtheria toxin (*DF-A*) was used for a negative selection. PCR primers are described under "Experimental Procedures." *B*, PCR analysis of genomic DNA derived from wild-type (*WT*) and LSST mutant mice. Using PCR primer sets of F1W/R1W and F1M/R1M (shown in *panel A*). *C–H*, frozen sections of peripheral (*C* and *F*), mesenteric (*D* and *G*), and Peyer's patches (*E* and *H*) from wild-type mice (*C–E*) or from LSST$^{\Delta}$ mice (*F–H*) were examined for L-selectin-IgM chimera binding using fluorescence microscopy. *Bar*, 50 μm. *I*, GlyCAM-1 was prepared from sera of wild-type and LSST$^{\Delta}$ mice, separated by SDS-polyacrylamide gel electrophoresis, and subjected to Western analysis using anti-GlyCAM-1 antibodies or the MECA-79 monoclonal antibody (*left panel*). The *right panel* shows the ratio of MECA-79 over GlyCAM-1, obtained by densitometric analysis of the *left panel*.

pounds can be separated by a shallow gradient elution using a Partisil SAX-10 column (29) or an Asahipak NH_2-bonded HPLC column as described previously (20). Oligosaccharides obtained after each step of sequential glycosidase digestion were also fractionated using the Asahipak column. For this, the sample was eluted for 10 min with a linear gradient from solvent A (64% acetonitrile, 36% H_2O) to a 70:30 mixture of solvent A and solvent B (64% acetonitrile, 36% 69 mM NaH_2PO_4/H_2O, pH 4.2), followed by a 40-min linear gradient elution to a 30:70 mixture of solvent A and solvent B. Finally, the sample was eluted for 5 min with a linear gradient elution to 100% of solvent B. Oligosaccharides were also digested by hexosaminidase A, which cleaves both non-sulfated and sulfated *N*-acetylglucosamine (30). Standard oligosaccharides were prepared from Chinese hamster ovary cells expressing LSST and Core1-β3GlcNAcT or Core2GlcNAcT-I or both.

Lymphocyte Homing—Lymphocyte homing *in vivo* was assayed as described previously (26, 31). Briefly, 2.5×10^7 5-chloromethyl fluorescein diacetate (CMFDA)-labeled lymphocytes from spleen and mesenteric lymph nodes, derived from wild-type mice, were injected into tail veins of 7- to 8-week-old wild-type, LSST$^{\Delta}$, Core2GlcNAcT$^{\Delta}$, and LSST$^{\Delta}$/Core2GlcNAcT$^{\Delta}$ mice. After 1 h, animals were sacrificed, and peripheral (axillary and cervical) and mesenteric lymph nodes, Peyer's patches, and spleen were isolated. Lymphocyte suspensions were prepared from these organs and subjected to fluorescence-activated cell sorting analysis to determine the fractional content of fluorescent cells.

Measurement of L-selectin-mediated Rolling on GlyCAM-1 Samples from Wild-type, LSST$^{\Delta}$, Core2GlcNAcT$^{\Delta}$, and LSST$^{\Delta}$/Core2GlcNAcT$^{\Delta}$ Mice—GlyCAM-1 was prepared from sera of wild-type, LSST$^{\Delta}$, Core2GlcNAcT$^{\Delta}$, and LSST$^{\Delta}$/Core2GlcNAcT$^{\Delta}$ mice, as described above, and captured on polystyrene plates, which had been coated with anti-GlyCAM-1 antibodies (20, 31). The amount of GlyCAM-1 from wild-type, LSST$^{\Delta}$, Core2GlcNAcT$^{\Delta}$, and LSST$^{\Delta}$/Core2GlcNAcT$^{\Delta}$ mice was adjusted to provide equivalent amounts of GlyCAM-1 as assessed by Western blotting analysis using the anti-GlyCAM-1 antibodies. Lymphocytes were initially introduced into the flow chamber at a wall shear stress of 5 dynes/cm^2 for 15 s, followed by the termination of flow, allowing cells to adhere under static conditions. Flow rate was then reinitiated at various shear forces. Image analysis was performed and analyzed as described (20, 32). At the same time, rolling velocities for individual cells (between 120 and 200 rolling cells per experiment) were determined for the results obtained on GlyCAM-1 isolated from wild-type and LSST$^{\Delta}$ mice as described previously (16).

In Situ Hybridization and Immunohistochemistry—The immunohistochemical staining of MECA-79 antigen and *in situ* hybridization for mouse Core1-β3GlcNAcT, Core2GlcNAcT, LSST, and FucT-VII were performed on the inflamed salivary gland of a 55-week-old NOD mouse as described previously (16, 20). Digoxigenin-labeled antisense and sense RNA probes were prepared by *in vitro* transcription from pGEM-3Zf(+) (Promega) containing a partial cDNA sequence of mouse Core1-β3GlcNAcT (nucleotides +705 to +854), Core2GlcNAcT (nucleotides +991 to + 1140), LSST (nucleotides +556 to +744), or FucT-VII (nucleotides +2196 to + 2497). Hybridized probes were detected by alkaline phosphatase-conjugated anti-digoxigenin antibody, and no specific signals were found in control experiments using sense probes.

Immunohistochemistry with the MECA-79 antibody was performed by the indirect immunoperoxidase method. Control experiments were done by omitting primary antibody from the procedure, and in this case no specific staining was seen. Counterstaining was carried out with hematoxylin.

RESULTS

Disruption of the Mouse LSST Locus—The gene encoding LSST was incorporated into a targeting vector by replacing a portion of the LSST gene with cDNAs encoding EGFP and the neomycin resistance enzyme. After homologous recombination, the resultant gene encodes the cytoplasmic, transmembrane, and stem regions of LSST (amino acid resides 1–32), which are fused with EGFP and driven by the LSST promoter (Fig. 1*A*). It

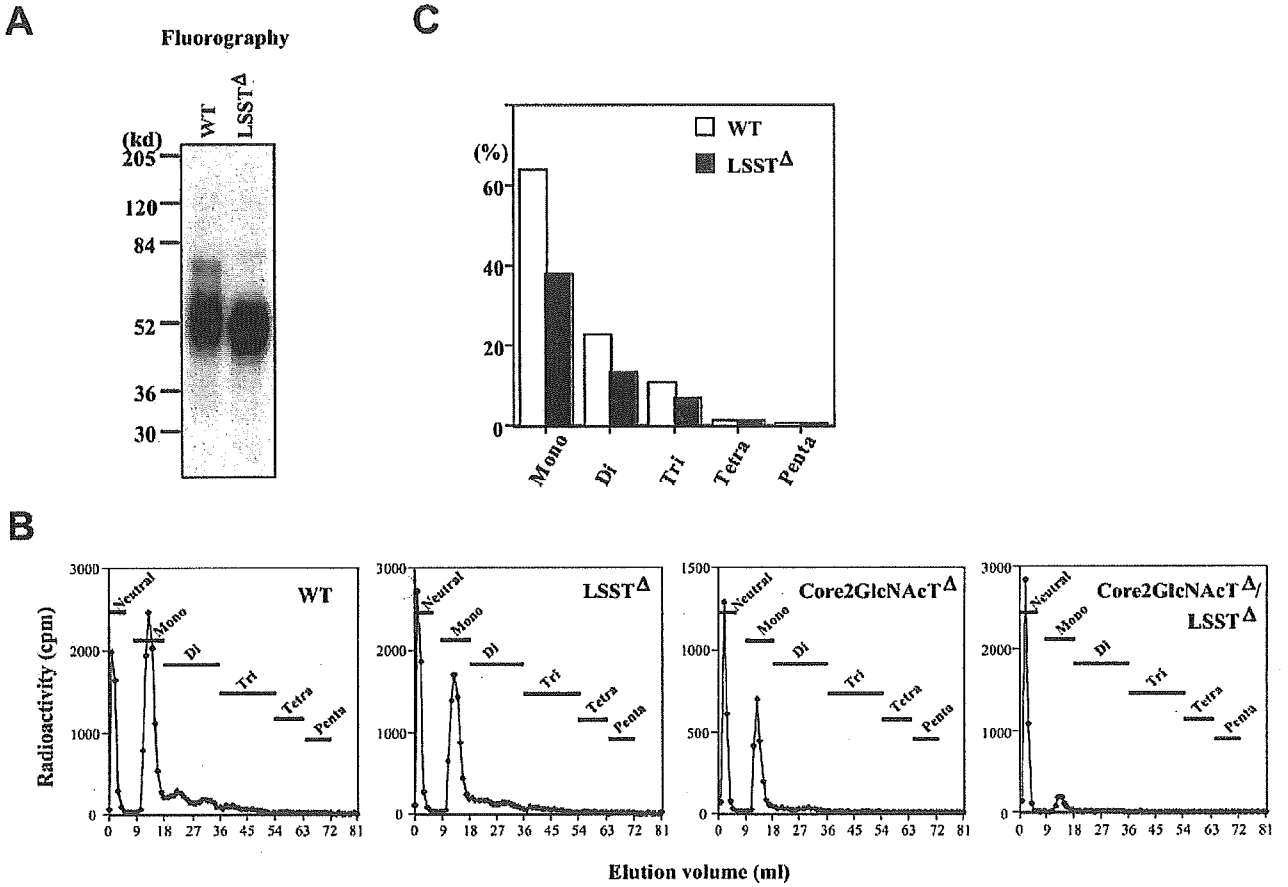

FIG. 2. **Oligosaccharide biosynthesis in LSST-deficient mice.** *A*, GlyCAM-1 purified from the culture medium derived from [^{3}H]galactose labeling of lymph nodes were subjected to SDS-PAGE followed by fluorography. *B*, *O*-linked oligosaccharides were isolated from glycoproteins shown in *panel A* and after removal of sialic acid, subjected to QAE-Sephadex column chromatography. Oligosaccharides eluting at the void volume represent unsulfated *O*-linked oligosaccharides, whereas monosulfated, disulfated, trisulfated, tetrasulfated, and pentasulfated *O*-linked oligosaccharides were eluted by increasing concentrations of NaCl. *C*, the amount of mono-, di-, tri-, tetra-, and pentasulfated *O*-linked oligosaccharides attached to GlyCAM-1 from wild-type and LSST$^{\Delta}$ mice; 100% = total sulfated *O*-linked oligosaccharides of GlyCAM-1 from wild-type mice.

has been shown that the cytoplasmic, transmembrane, and stem regions of Golgi-associated enzymes specify Golgi retention (33, 34), and thus the fused protein is expected to be transported to the same Golgi compartment as the intact LSST.

Targeted ES cell clones were injected into C57BL/6 blastocysts, and F1 crosses of chimeric mice produced LSST$^{\Delta}$ as determined by PCR of genomic DNA (Fig. 1*B*). Intercrosses of heterozygous progeny yielded litters of normal size with Mendelian transmission of the null allele.

L-selectin Ligand Expression in HEV of LSST$^{\Delta}$ Mice—LSST$^{\Delta}$ mice did not show a detectable anomaly in the abundance or anatomy of HEV in the secondary lymphoid organs, compared with genetically matched wild-type mice. However, the binding of L-selectin-IgM chimeric protein was almost entirely lost on the luminal side of HEV derived from peripheral and mesenteric lymph nodes under the conditions where strong binding was observed in HEV of wild-type mice (Fig. 1, *C* and *F*). Only a residual binding was detected on the intraluminal surface of the bottom layer of high endothelial cells in LSSTΔ mouse HEV (Fig. 1*F*). However, a more prominent binding of L-selectin-IgM chimeric protein persisted at the bottom layer of high endothelial cells in HEV even after inactivation of LSST (Fig. 1, *F–H*). This layer is called the abluminal lining hereafter. The abluminal expression of L-selectin ligand is also present on Peyer's patches of wild-type mice (Fig. 1*E*). Consistent with these findings, MECA-79 antigen is drastically reduced in GlyCAM-1 isolated from LSST$^{\Delta}$ mice, and only 34% of MECA-79 antigen was detected compared with GlyCAM-1 from wild-type mice (Fig. 1*I*). These results combined strongly suggest that the great majority of 6-sulfo sLe^x on the luminal region of HEV is dependent on LSST, whereas the majority of L-selectin ligand, including 6-sulfo sLe^x in the abluminal lining of lymph nodes and Peyer's patches, is synthesized by a sulfotransferase other than LSST.

GlyCAM-1 Derived from LSST$^{\Delta}$ Mice Still Contains Significant Amounts of 6-Sulfo sLe^x—The above results suggest that levels of L-selectin ligand in peripheral and mesenteric lymph nodes should be significantly reduced, and only a small fraction of GlyCAM-1 *O*-glycans should contain 6-sulfo sLe^x. Because no structural information was available on GlyCAM-1 from LSST$^{\Delta}$ mice in the previous report (23), we analyzed *O*-glycans attached to GlyCAM-1 isolated from peripheral and mesenteric lymph nodes cultured in the presence of [^{3}H]galactose as described previously (Fig. 2*A*) (20). Mucin-type *O*-glycans prepared from the GlyCAM-1 samples of wild-type mice contained a significant amount of sulfated *O*-glycans, which were bound and eluted from a QAE-Sephadex column, whereas appreciable loss of sulfated *O*-glycans was noted for GlyCAM-1 from LSST$^{\Delta}$ mice (Fig. 2*B*).

These oligosaccharides were further analyzed using gel filtration and HPLC as described previously (16, 20). 6-Sulfo sLe^x was reduced in all of GlyCAM-1 *O*-glycans isolated from LSST$^{\Delta}$ mice than wild-type mice (Fig. 2*C*). In particular, 6-sulfo sLe^x in extended core 1 *O*-glycans (shown in *orange* in Fig. 3) is

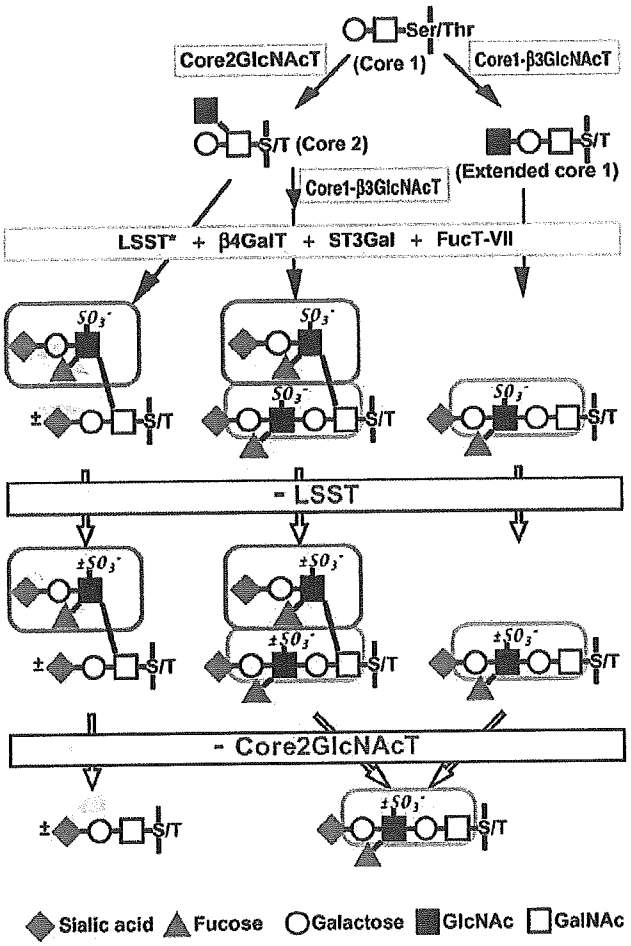

FIG. 3. **Structure and biosynthesis of L-selectin ligand oligosaccharides.** Core 1 *O*-glycan can be extended by Core1-β3GlcNAcT, sulfated by LSST, then galactosylated to form the minimum epitope for the MECA-79 antibody (shown in the *orange circle*). The galactosylated oligosaccharide is further sialylated and fucosylated to form 6-sulfo sLe^x in extended core 1 *O*-glycans (*right*). Core 1 oligosaccharide can be converted to core 2 *O*-glycan by Core2GlcNAcT, sulfated by LSST, galactosylated, sialylated, and fucosylated to form 6-sulfo sLe^x in core 2-branched *O*-glycans (shown in the *magenta circle* at *left*). Core 1-β3GlcNAcT can act on core 2-branched *O*-glycans, leading to biantennary *O*-glycans containing both core 2 branch and core 1 extension. By contrast, Core2GlcNAcT cannot act on extended core 1 *O*-glycans (20). One or both of these branches can be modified to contain 6-sulfo sLe^x (*middle*). All of these processed *O*-glycans function as L-selectin ligands. These schematic structures correspond to *Structure 1* (*left*), *Structure 2* (*right*), and *Structures 3–5* (*middle*) shown in Fig. 5. In addition to LSST, GlcNAc6ST-1 likely forms 6-sulfo *N*-acetylglucosamine in HEV. After inactivation of LSST (*−LSST*), the majority of 6-sulfate in extended core1 is abolished. After further inactivation of Core2GlcNAcT (*−Core2GlcNAcT*), the majority of *O*-glycans is either core 1 *O*-glycans (*bottom left*) or extended core 1 *O*-glycans containing sLe^x (*bottom right*). *β4GalT*, β1,4-galactosyltransferase (52); *ST3Gal*, α2,3-sialyltransferase (53); *FucT-VII*, fucosyltransferase VII.

almost absent (see after inactivation of LSST, *−LSST* in Fig. 3). This finding is consistent with the above finding that the MECA-79 epitope was dramatically diminished in GlyCAM-1 from LSST$^\Delta$ mice. Most of the remaining 6-sulfo sLe^x on mucin-type *O*-glycans in HEV was found in core 2-branch (shown in *magenta* in Fig. 3, see below for detailed structural analysis). Core 2 branch in HEV is synthesized exclusively by Core2GlcNAcT (20). These results thus prompted us to generate double knockout mice deficient in both LSST and Core2GlcNAcT to determine the *in vivo* roles of 6-sulfo sLe^x as L-selectin ligands.

Loss of L-selectin Ligands and 6-Sulfo sLe^x in Double Knockout Mice Deficient in Both LSST and Core2GlcNAcT—To cross-breed the mice, both LSST null mice and Core2GlcNAcT null mice were separately back-crossed with C57BL/6. Cross-breeding of C57BL/6-LSST$^\Delta$ and C57BL/6-Core2GlcNAcT$^\Delta$ produced LSST$^\Delta$/Core2GlcNAcT$^\Delta$ mice with Mendelian transmission of the null allele (Fig. 4*A*). Double knockout mice exhibited no anomalies in gross morphology, were fertile, and were not susceptible to endogenous microbes in a regular pathogen-free environment.

Examination of lymph nodes showed that binding of L-selectin-IgM chimera to HEV was decreased in Core2GlcNAcT$^\Delta$ mice, whereas no appreciable loss of MECA-79 antigen was observed (Fig. 4*B*). On the other hand, LSST$^\Delta$/Core2GlcNAcT$^\Delta$ mice exhibited substantially decreased binding of L-selectin-IgM chimera to HEV and negligible amount of MECA-79 antigen at the luminal side of HEV (Fig. 4*B*). This loss in L-selectin ligand and MECA-79 antigen at the luminal side of the lymph nodes was associated with expression of LSST-GFP protein. These results establish that LSST and Core2GlcNAcT are primarily responsible for L-selectin ligand expression on the luminal side of HEV.

Structural analysis of GlyCAM-1 was carried out to define the chemical nature of the sulfated oligosaccharides. Core2GlcNAcT$^\Delta$ mice contained much less sulfated *O*-glycans in GlyCAM-1, which were retained and eluted from a QAE-Sephadex column, than wild-type mice (Fig. 2*B*). Furthermore, a dramatic reduction in sulfated *O*-glycans was observed for GlyCAM-1 derived from LSST$^\Delta$/Core2GlcNAcT$^\Delta$ mice. The sulfated oligosaccharide fractions isolated by QAE-Sephadex column chromatography were then subjected to Bio-Gel P-4 gel filtration, sequentially digested with specific glycosidases, and analyzed by Bio-Gel P-4 gel filtration and HPLC using an NH_2-bonded column as described in previous studies (16, 20). These structural analyses of *O*-glycans derived from wild-type, LSST$^\Delta$, Core2GlcNAcT$^\Delta$, and LSST$^\Delta$/Core2GlcNAcT$^\Delta$ mice revealed the oligosaccharide structures shown in Fig. 5*A*. In GlyCAM-1 from wild-type mice, the majority of 6-sulfo sLe^x is contained in core 2-branched *O*-glycans (Fig. 5*A*, *Structure 1*), extended core 1 *O*-glycans (*Structure 2*), monosulfated bi-antennary *O*-glycans (*Structure 3* and *4*), and disulfated bi-antennary *O*-glycans (*Structure 5*) (Fig. 5*A*). In GlyCAM-1 from LSST$^\Delta$ mice, MECA-79-positive *Structure 2* is dramatically decreased and MECA-79-positive *Structures 4* and *5* are also decreased. These results are consistent with the above findings that LSST$^\Delta$ mice express a negligible amount of luminal MECA-79 antigen. In GlyCAM-1 derived from Core2GlcNAcT$^\Delta$ mice, *Structures 1*, *3*, *4*, and *5* containing core 2 branch are absent, whereas MECA-79-positive *Structure 2*, which contains core 1 extension alone, increases (Fig. 5, *A* and *B*).

In GlyCAM-1 derived from LSST$^\Delta$/Core2GlcNAcT$^\Delta$ double null mice, the amount of oligosaccharides containing 6-sulfo sLe^x in extended core 1 (*Structures 3–5*) is further decreased and only a small amount of *Structure 2* remains, when intraluminal MECA-79 antigen is almost absent (Fig. 4*B*). These results suggest that the majority of MECA-79 antigen in wild-type mice is carried by *Structures 3–5*. At the same time, the amount of non-sulfated sLe^x in LSST$^\Delta$/Core2GlcNAcT$^\Delta$ mice is increased to 18.7% of total *O*-glycans compared from 11% of those in Core2GlcNAcT$^\Delta$ mice (data not shown). These results indicate that the loss of 6-sulfo sLe^x is compensated for by the increase of non-sulfated sLe^x in LSST$^\Delta$/Core2GlcNAcT$^\Delta$ mice. These results also indicate that LSST is mainly responsible for 6-sulfation at extended core 1 *O*-glycans, whereas a sulfotransferase other than LSST contributes to 6-sulfation at core 2-branch in addition to LSST.

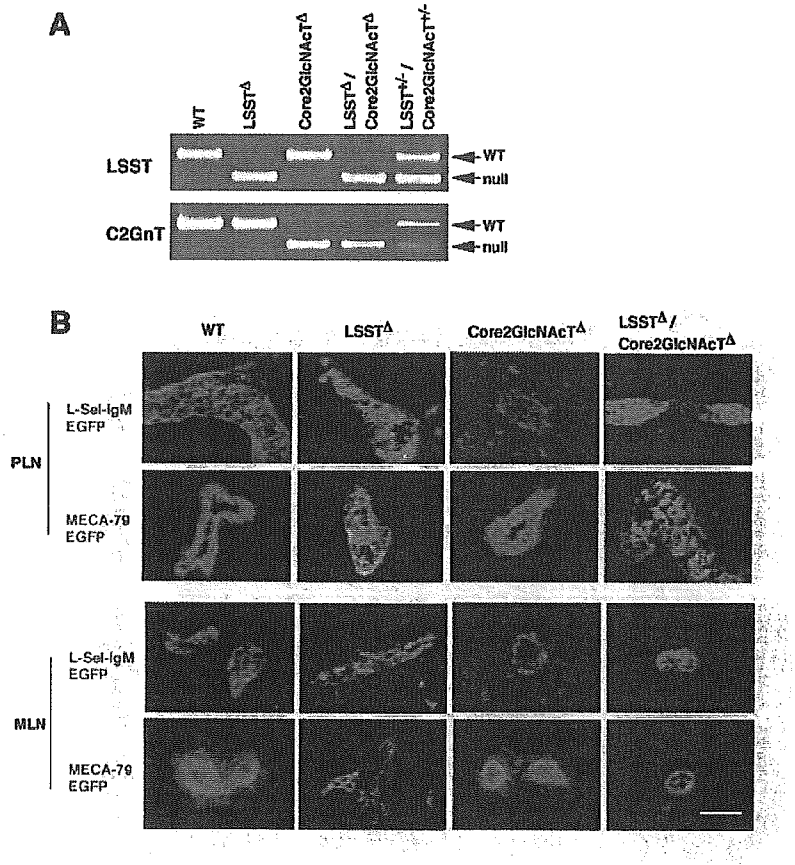

FIG. 4. **Inactivation of both LSST and Core2GlcNAcT.** *A*, cross-breeding of LSST$^{\Delta}$ mice with Core2GlcNAcT$^{\Delta}$ mice. Genomic DNA of mice was analyzed by PCR, which yielded products of correct sizes (479 bp for wild-type (*WT*) and 224 bp for null allele). *B*, expression of L-selectin ligand and MECA-79 antigen in HEV of lymph nodes from wild-type, LSST$^{\Delta}$/Core2GlcNAcT$^{\Delta}$, and LSST$^{\Delta}$/Core2GlcNAcT$^{\Delta}$ mice. Staining is shown for L-selectin-IgM binding or MECA-79 antigen (*red*) and expression of LSST-EGFP (*green*). *PLN*, peripheral lymph nodes; *MLN*, mesenteric lymph nodes. *Bar*, 50 μm.

Defective Lymphocyte Homing in LSST$^{\Delta}$/Core2GlcNAcT$^{\Delta}$ Mice—To determine the role of LSST and Core2GlcNAcT in L-selectin ligand activity at HEV, a lymphocyte homing assay was carried out on wild-type, LSST$^{\Delta}$, Core2GlcNAcT$^{\Delta}$, or LSST$^{\Delta}$/Core2GlcNAcT$^{\Delta}$ mice. Homing of wild-type lymphocytes to the peripheral and mesenteric lymph nodes of LSST$^{\Delta}$- or Core2GlcNAcT$^{\Delta}$-recipient mice was decreased to 55 and 85%, respectively, relative to homing in wild-type-recipient mice (Fig. 6*A*). The number of lymphocytes in the peripheral lymph nodes was decreased to 60% in LSST$^{\Delta}$ mice and 78% in Core2GlcNAcT$^{\Delta}$ mice (Fig. 6*B*). By inactivating both LSST and Core2GlcNAcT, a dramatic decrease in lymphocyte homing to peripheral lymph nodes and mesenteric lymph nodes was observed (Fig. 6*A*). The remaining lymphocyte homing activity in the peripheral lymph nodes of LSST$^{\Delta}$/Core2GlcNAcT$^{\Delta}$ mice still depended on L-selectin-mediated adhesion, because anti-L-selectin antibody treatment of lymphocytes completely abolished lymphocyte homing (Fig. 6*A*). This complete inhibition is equivalent to that observed in mice deficient in L-selectin (35) or mice deficient in both FucT-VII and FucT-IV (31). Lymphocyte numbers in the peripheral lymph nodes of double knockout mice were decreased to 40% relative to that of wild-type mice, whereas only a small decrease was observed in lymphocyte numbers in mesenteric lymph nodes of the same mutant mice (Fig. 6*B*). These results in combination suggest that the efficiency of lymphocyte homing is in proportion to the amount of 6-sulfo sLe^x, regardless of whether 6-sulfo sLe^x is present on extended core 1 or core 2 branch structure.

Loss of 6-Sulfo sLe^x Leads to Increase in the Velocity of Rolling Lymphocytes—To further determine the roles of L-selectin ligands directed by LSST and Core2GlcNAcT, wild-type lymphocytes were rolled over plates that had been coated with GlyCAM-1 prepared from the sera of wild-type, LSST$^{\Delta}$, Core2GlcNAcT$^{\Delta}$, and LSST$^{\Delta}$/Core2GlcNAcT$^{\Delta}$. Surprisingly, GlyCAM-1 from LSST$^{\Delta}$ mice exhibited only a marginal decrease in L-selectin ligand activity compared with wild-type mice (Fig. 6*C*). By contrast, rolling on GlyCAM-1 from Core2GlcNAcT$^{\Delta}$ mice was decreased significantly compared with that seen in wild-type GlyCAM-1. GlyCAM-1 from double knockout LSST$^{\Delta}$/Core2GlcNAcT$^{\Delta}$ mice supported the least amount of lymphocyte rolling (Fig. 6*C*).

The above results suggest, however, that the role of 6-sulfo sLe^x was not precisely measured by examining the number of tethering and rolling lymphocytes, because only a marginal decrease was observed on GlyCAM-1 derived from LSST$^{\Delta}$ mice. We thus measured the velocity of rolling lymphocytes, because we previously found that the effect of 6-sulfation on L-selectin ligand is measured best by examining the velocity of rolling lymphocytes (16). GlyCAM-1 from wild-type mice yielded an average velocity of 18 μm/s at a shear stress of 2.32 dyne/cm^2, whereas GlyCAM-1 from LSST$^{\Delta}$ yielded ~31 μm/s at the same shear stress (Fig. 6*D*). These results indicate that 6-sulfation on sLe^x dramatically decreases the velocity of rolling lymphocytes. By contrast, the number of rolling lymphocytes on LSST$^{\Delta}$ GlyCAM-1 did not decrease at the same shear force and decreased only by 35% under weaker shear forces (Fig. 6*C*). These results suggest that 6-sulfation facilitates lymphocyte homing mainly by decreasing the velocity of rolling lymphocytes.

Coordinate Expression of LSST, Core2GlcNAcT, Core1-β3GlcNAcT, and FucT-VII in HEV-like Microvasculature of NOD Mice—L-selectin ligand-positive HEV is constitutively present in secondary lymphoid organs. By contrast, conversion of flat walled vascular endothelium to a HEV-like morphology is observed in association with certain inflammatory and preneoplastic conditions. A well characterized such example, the NOD mouse, displays HEV-like structures in pancreatic islets and inflammatory salivary glands. In these organs, recruitment of lymphocytes through L-selectin ligand leads to β-cell

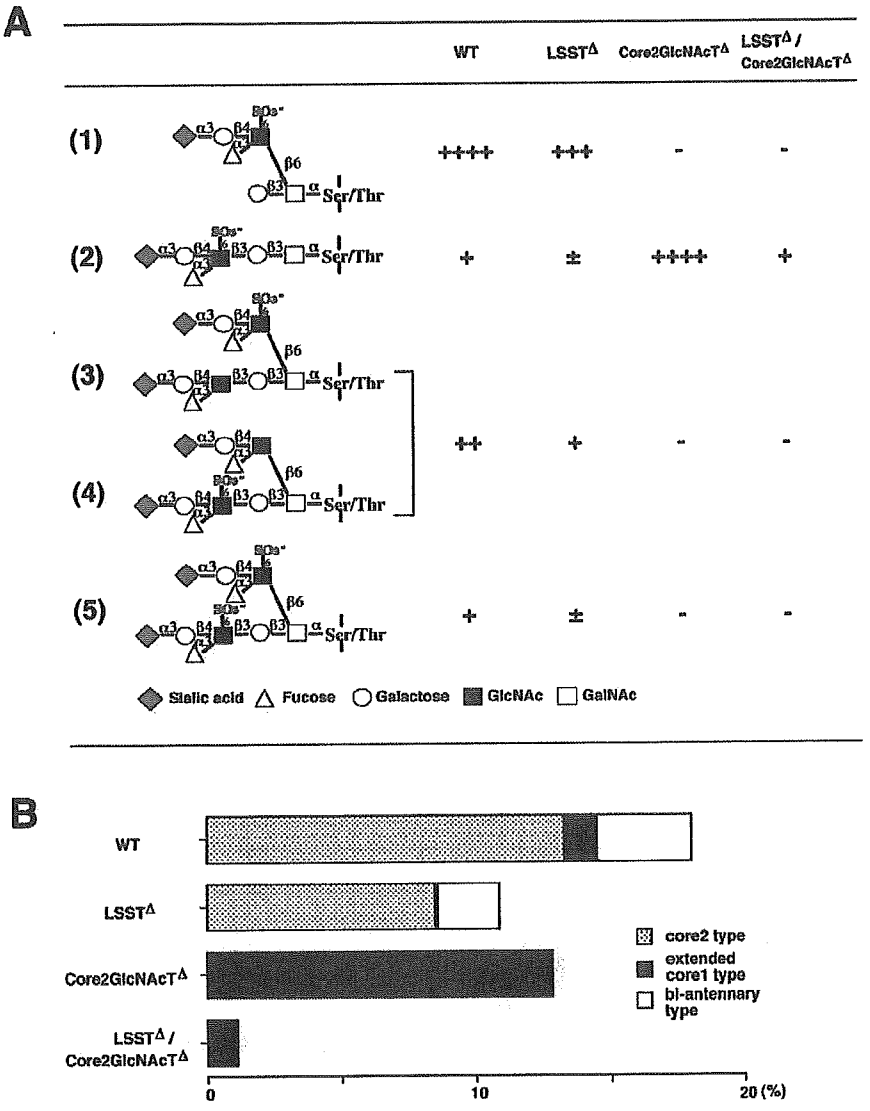

FIG. 5. **Structures of major sulfated *O*-linked oligosaccharides attached to GlyCAM-1 from wild-type, LSST$^{\Delta}$, Core2GlcNAcT$^{\Delta}$, and LSST$^{\Delta}$/Core2-GlcNAcT$^{\Delta}$ mice.** *A*, the structures of oligosaccharides containing 6-sulfo sLe^{x} in GlyCAM-1 derived from HEV were determined and shown. *B*, the amount of core 2-branched *O*-glycans (*Structure 1*), extended core 1 *O*-glycans (*Structure 2*), and biantennary *O*-glycans (*Structure 3–5*), which contain 6-sulfo sLe^{x}, is shown. 100% = total *O*-glycans that include non-sialylated and non-sulfated *O*-glycans.

destruction and sialoadenitis of salivary glands (5, 6). *In situ* hybridization shows that LSST and Core2GlcNAcT are transcribed in HEV-like MECA-79-positive structures in salivary glands of NOD mice (Fig. 7). These transcripts colocalize in adjacent sections with transcripts for Core1-β3GlcNAcT, FucT-VII, and Core2GlcNAcT, although the expression level of Core2GlcNAcT transcripts is apparently lower than that of the others (Fig. 7). These results imply that LSST, Core1-β3GlcNAcT, FucT-VII, and to a lesser extent Core2GlcNAcT contribute to induction of L-selectin ligands in HEV-like structures present in inflamed salivary glands of the NOD mouse.

DISCUSSION

Intense interest in the analysis of oligosaccharides elaborated by HEV has been shown in an attempt to understand the role of L-selectin-mediated adhesion in lymphocyte homing. Attempts to answer this question by ablating counterreceptors such as GlyCAM-1 and CD34 have not been useful in defining these oligosaccharides due to the number of highly glycosylated HEV proteins, which carry the same functional oligosaccharides (3, 36). By contrast, deletion of FucT-VII or fucosyltransferase IV (FucT-IV) or their double mutant has yielded useful information indicating an absolute requirement of α1,3-linked fucose for L-selectin ligand activity (26, 31). To define oligosaccharide elements other than fucose, we have inactivated a key sulfotransferase (LSST) that forms 6-sulfo *N*-acetylglucosamine in the context of 6-sulfo sLe^{x}, a major ligand for L-selectin. LSST$^{\Delta}$ mice, however, exhibited substantial residual L-selectin ligand activity at HEV, despite the fact that the LSST$^{\Delta}$ mice lost almost all luminal expression of 6-sulfo sLe^{x} in extended core 1 *O*-glycans. These results agree in principle with the previous report on mutant mice deficient in LSST (23). Considering that 6-sulfo sLe^{x} and possibly sLe^{x} on core 2-branched *O*-glycans most likely contribute to the remaining L-selectin ligand activity at HEV, we have generated LSST$^{\Delta}$/Core2GlcNAcT$^{\Delta}$ double null mice by cross-breeding LSST$^{\Delta}$ mice with Core2GlcNAcT$^{\Delta}$ mice. These studies reveal that LSST and Core2GlcNAcT, which form 6-sulfo *N*-acetylglucosamine and core 2-branch, respectively, control L-selectin ligand synthesis in a cooperative manner.

The present study demonstrates that a large portion of L-selectin ligand, 6-sulfo sLe^{x} on HEV, is capped on core 2-branched *O*-glycans. Deletion of Core2GlcNAcT resulted in a significant loss of lymphocyte homing activity and an appreciable decrease in lymphocyte numbers in peripheral lymph

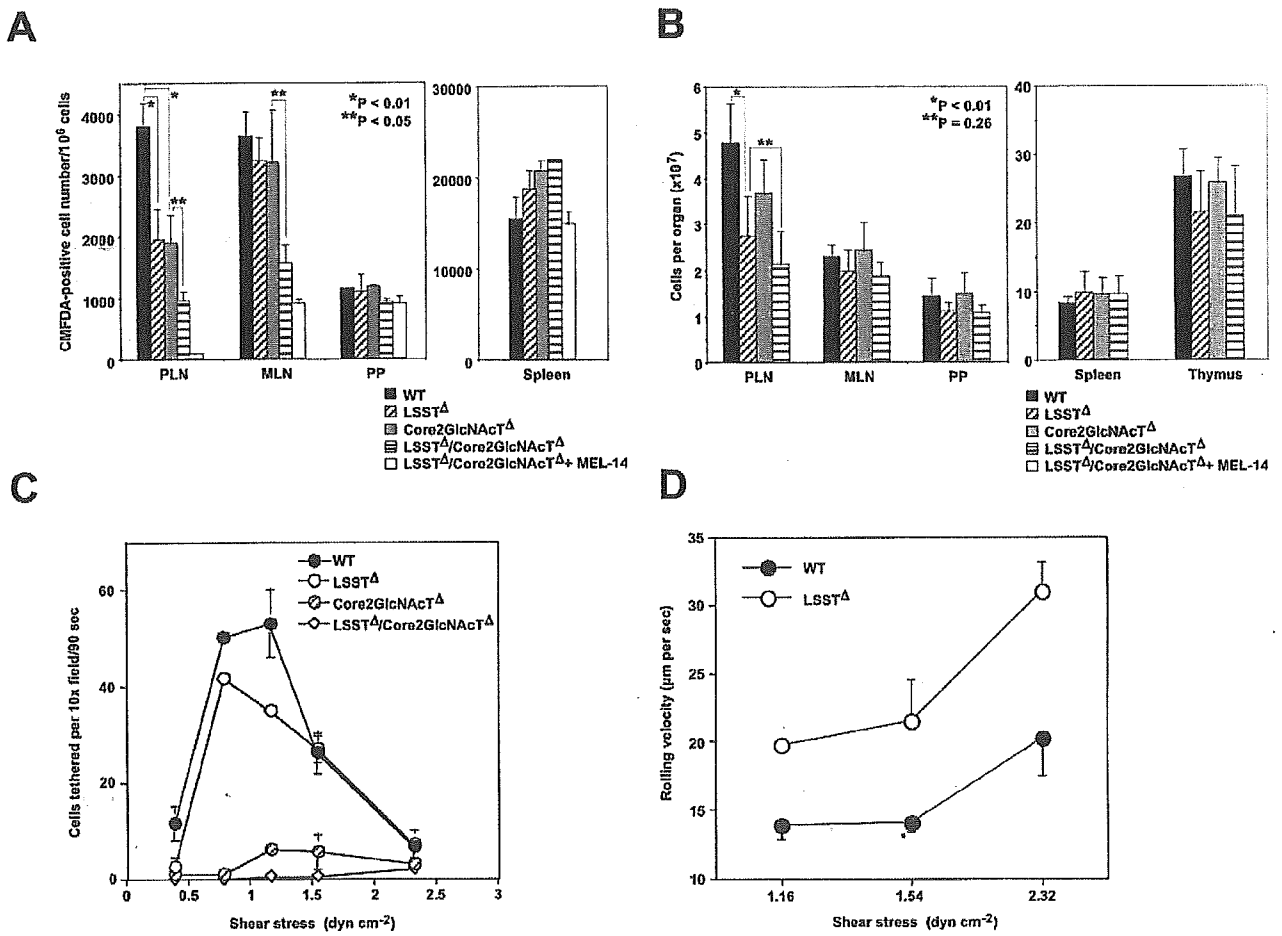

FIG. 6. **Lymphocyte homing and selectin ligand expression in wild-type LSST$^{\Delta}$, Core2GlcNAcT$^{\Delta}$, and LSST$^{\Delta}$/Core2GlcNAcT$^{\Delta}$ mice.** *A*, CMFDA-labeled lymphocytes from mesenteric lymph nodes and spleens of wild-type mice were injected into the tail vein of different mouse strains. Mice were sacrificed 1 h later, and fluorescent lymphocytes in lymphocyte suspensions from lymphoid organs were quantitated by flow cytometry. Residual lymphocyte homing to peripheral lymph nodes in LSST$^{\Delta}$/Core2GlcNAcT$^{\Delta}$ mice was completely abolished by anti-L-selectin antibody (MEL-14) treatment of lymphocytes before the lymphocyte injection. At least four recipient mice were tested for each experiment. *B*, lymphocytes recovered from different lymphoid organs of 7-week-old mice were quantitated. *C* and *D*, lymphocyte rolling using a flow chamber coated with GlyCAM-1 isolated from different strains. The number of adhering lymphocytes is shown for all four mouse strains (*C*), whereas the average rolling velocity of lymphocytes is shown for wild-type and LSST$^{\Delta}$-recipient mice (*D*). In *A–D*, two independent experiments yielded almost identical results and results from one experiment are shown.

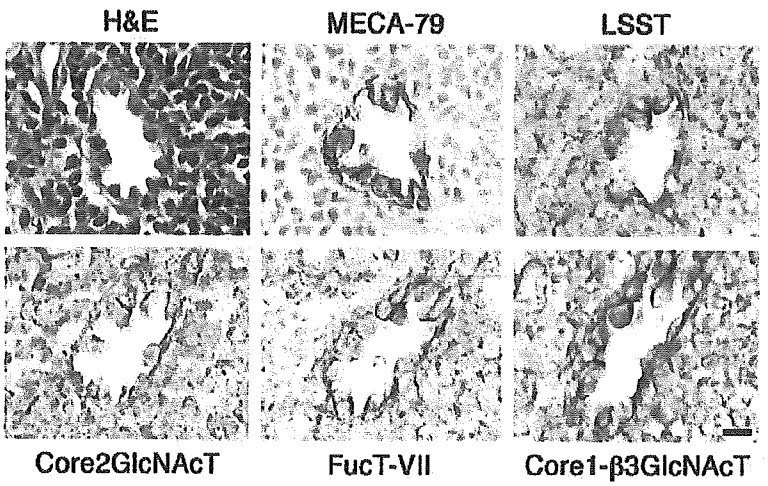

FIG. 7. **Co-localized expression of MECA-79 antigen, LSST, Core2-GlcNAcT, Core1-β3GlcNAcT, and FucT-VII in a HEV-like vessel in the salivary gland of NOD mice.** HEV-like vessels were found in the salivary glands of 55-week-old NOD mice, which developed sialoadenitis accompanying marked lymphocyte infiltration. Serial sections of the representative site were subjected to immunochemistry using the MECA-79 antibody and *in situ* hybridization using antisense probes for mouse LSST, Core2GlcNAcT, FucT-VII, and Core1-β3GlcNAcT. *Bar*, 10 μm.

nodes. These results are, however, slightly different from those obtained in the previous report (25). In the present study, we made efforts to obtain a similar genetic background for LSST$^{\Delta}$ and Core2GlcNAcT$^{\Delta}$ mice by cross-breeding Core2GlcNAcT$^{\Delta}$ and LSST$^{\Delta}$ mice with C57BL/6. Those resultant Core2-GlcNAcT$^{\Delta}$ and LSST$^{\Delta}$ mice were then cross-bred to generate

LSST$^{\Delta}$/Core2GlcNAcT$^{\Delta}$ double knockout mice. For lymphocyte homing assay, lymphocytes from mesenteric lymph nodes and spleen were used in the present study, whereas mesenteric lymphocytes were used in the previous study (25). This difference may cause a different homing profile. In this aspect, it is noteworthy that the previous studies showed a decrement in both lymphocyte homing activity and lymphocyte numbers in the secondary lymphoid organs for Core2GlcNAcT null mice, although it was judged to be statistically insignificant (25). Recently, it has been shown that 6-sulfo sLe^x on bi-antennary *O*-glycans is a better L-selectin ligand than 6-sulfo sLe^x on *O*-glycans containing core 1 extension or core 2-branch alone (20). Core2GlcNAcT$^{\Delta}$ mice entirely lack core 2-branch in HEV L-selectin ligands and such a synergistic effect cannot be achieved in Core2GlcNAcT$^{\Delta}$ mice. This may explain why Core2GlcNAcT$^{\Delta}$ mice exhibit a reduced lymphocyte homing activity relative to wild-type mice.

Stamaa *et al.* (37) reported the presence of 6-sulfo sLe^x on extended core 1 in CD34 isolated from human tonsil. However, the method employed in their study cannot differentiate 6-sulfo sLe^x in extended core 1 *O*-glycan from 6-sulfo sLe^x in core 2-branched *O*-glycan, because no tandem mass spectrometry analysis was performed. Further studies are thus necessary to determine if extended core 1 *O*-glycans (in particular, *Structure 4* in Fig. 5) are present with significant quantity in human tonsil HEV.

Although LSST is concluded to play a critical role in the biosynthesis of 6-sulfo sLe^x at the luminal side of HEV, inactivation of LSST did not lead to loss of L-selectin ligand at the abluminal side of HEV. The abluminal expression of L-selectin ligand and MECA-79 antigen, which constitutes a portion of L-selectin ligand, has been previously reported (21), but has not been studied further. The majority of L-selectin ligand and MECA-79 antigen in the peripheral lymph nodes is strongly expressed on the luminal side of HEV, which has obscured the abluminal L-selectin ligand of the peripheral lymph nodes. However, the abluminal side of Peyer's patches in wild-type mice is also decorated by MECA-79 antigen and L-selectin ligands, which are retained in LSST$^{\Delta}$ mice. In Peyer's patches, it has been shown that L-selectin plays a limited but definite role in the tethering and rolling of lymphocytes, presumably by adhering to L-selectin ligands at the luminal sides of HEV (38, 39). However, this MECA-79-negative L-selectin ligand appears to be relatively weak, because the binding of L-selectin-IgM chimeric protein was not observed at the luminal side of Peyer's patches in both wild-type and LSST$^{\Delta}$ mice (Fig. 1, *E* and *H*). Moreover, L-selectin-mediated lymphocyte homing in Peyer's patches can be compensated with relative ease by other adhesion mechanisms, because anti-L-selectin antibody treatment had a minimum effect on the lymphocyte homing to Peyer's patches (Fig. 6*A*). It is not apparent if this limited role of L-selectin ligand activity on the luminal side of Peyer's patches is supplemented by the presence of abluminal L-selectin ligands.

Our studies also demonstrate that a small amount of 6-sulfo sLe^x is present on extended core 1 *O*-glycans attached to GlyCAM-1 isolated from HEV of LSST$^{\Delta}$/Core2GlcNAcT$^{\Delta}$ mice (Fig. 5*B*). This finding indicates that there must be another sulfotransferase that adds a 6-sulfate group in the context of extended core 1, thus forming the MECA-79 epitope as well. It is also possible that 6-sulfo sLe^x in the abluminal side of HEV after inactivation of LSST may contribute to some of the remaining 6-sulfo sLe^x detected on GlyCAM-1 released from HEV. GlcNAc-6-*O*-sulfotransferase-1 (GlcNAc6ST-1) was shown to form the MECA-79 epitope (40, 41) and thus 6-sulfo sLe^x on extended core 1 *O*-glycans. Because GlcNAc6ST-1 is also expressed in HEV (16, 42), these combined results strongly suggest that GlcNAc6ST-1 also contributes to formation of 6-sulfo sLe^x on HEV in addition to LSST.

The same results also demonstrate that a significant portion of lymphocyte homing to the peripheral lymph nodes remains after inactivation of both LSST and Core2GlcNAcT. This remaining L-selectin ligand activity is apparently more than that expected from residual 6-sulfo sLe^x present in LSST$^{\Delta}$/Core2GlcNAcT$^{\Delta}$ mice. As shown recently, non-sulfated sLe^x on extended core 1 *O*-glycans serves as an L-selectin ligand, although it is not as good a ligand as sLe^x on core 2-branched *O*-glycans (43–45). Because LSST$^{\Delta}$/Core2GlcNAcT$^{\Delta}$ mice contain non-sulfated sLe^x in 18.7% of total *O*-glycans, it is likely that non-sulfated sLe^x on extended core 1 *O*-glycans contributes to this remaining L-selectin ligand. It is also possible that this remaining L-selectin ligand activity may be derived from L-selectin counterreceptors resistant to *O*-glycoprotease (46), which cleaves the majority of glycoproteins that contain mucin type *O*-glycans. This class of MECA-79-negative L-selectin ligand might include heparan sulfate (47, 48) and may play a role in lymphocyte homing.

The transcripts of Core2GlcNAcT and Core1-β3GlcNAcT are expressed in HEV, but they were also detected in wide variety of cells, including colon, lymphocytes, and neutrophils (20, 43, 49, 50). Similarly, the transcripts of FucT-VII are expressed in neutrophils, in addition to HEV (43, 51). In salivary glands of NOD mice, LSST, Core2GlcNAcT, Core1-β3GlcNAcT, and FucT-VII are expressed in HEV-like microvasculature, which is decorated by MECA-79 antigen. Similarly, it was shown that LSST and FucT-VII transcripts were expressed in MECA-79-positive HEV-like microvasculature in hyperplastic thymus of the AKR mouse (16). These observations suggest that LSST, FucT-VII, and in some instances Core1-β3GlcNAcT and Core2GlcNAcT are up-regulated in the formation of HEV and HEV-like structures, and coordinated regulation of these enzymes directs synthesis of L-selectin ligands. The observations on inflamed salivary glands of NOD mice, hyperplastic thymus of AKR mice and HEV in lymph nodes of wild-type mice also suggest that among these enzymes, LSST is most restricted to HEV, and that the up-regulation of LSST may be critical for induction of L-selectin counterreceptors on HEV-like microvasculature in chronic inflammation.

In conclusion, our observations demonstrate that Core2GlcNAcT and HEV-restricted LSST collaboratively control synthesis of L-selectin ligands in HEV. Expression of LSST and Core2GlcNAcT was also observed in HEV-like vasculature formed in inflamed salivary glands of NOD mice. These findings as a whole indicate that LSST and Core2GlcNAcT together provide a major contribution to synthesis of HEV-borne L-selectin ligands, to lymphocyte homing to secondary lymphoid organs, and to lymphocyte trafficking associated with transformation of flat wall vasculature into HEV-like vessels under pathological conditions.

Acknowledgments—We thank Dr. Steven Rosen for the kind gift of rabbit anti-GlyCAM-1 antibodies; Drs. Eugene Butcher, James Dennis, and Michiko Fukuda for useful discussions; and Dr. Elise Lamar for organizing the manuscript.

REFERENCES

1. Springer, T. A. (1994) *Cell* **76,** 301–314
2. Butcher, E. C., and Picker, L. J. (1996) *Science* **272,** 60–66
3. Kansas, G. S. (1996) *Blood* **88,** 3259–3287
4. von Andrian, U. H., and Mackay, C. R. (2000) *N. Engl. J. Med.* **343,** 1020–1034
5. Hanninen, A., Taylor, C., Streeter, P. R., Stark, L. S., Sarte, J. M., Shizuru, J. A., Simell, O., and Michie, S. A. (1993) *J. Clin. Invest.* **92,** 2509–2515
6. Faveeuw, C., Gagnerault, M. C., and Lepault, F. (1994) *J. Immunol.* **152,** 5969–5978
7. Tururnen, J. P., Majuri, M. L., Seppo, A., Tiisala, S., Paavonen, T., Miyasaka, M., Lemstrom, K., Penttila, L., Renkonen, O., and Renkonen, R. (1995) *J. Exp. Med.* **182,** 1133–1141

8. Toppila, S., Paavonen, T., Nieminen, M. S., Hayry, P., and Renkonen, R. (1999) *Am. J. Pathol.* **155,** 1303–1310
9. Salmi, M., Granfors, K., MacDermott, R., and Jalkanen, S. (1994) *Gastroenterology* **106,** 596–605
10. van Dinther-Janssen, A. C., Pals, S. T., Scheper, R., Breedveld, F., and Meijer, C. J. (1990) *J. Rheumatol.* **17,** 11–17
11. Michie, S. A., Streeter, P. R., Bolt, P. A., Butcher, E. C., and Picker, L. J. (1993) *Am. J. Pathol.* **143,** 1688–1698
12. Michie, S. A., Streeter, P. R., Butcher, E. C., and Rouse, R. V. (1995) *Am. J. Pathol.* **147,** 412–421
13. Rosen, S. D. (1999) *Am. J. Pathol.* **155,** 1013–1020
14. Imai, Y., Lasky, L. A., and Rosen, S. D. (1993) *Nature* **361,** 555–557
15. Hemmerich, S., Leffler, H., and Rosen, S. D. (1995) *J. Biol. Chem.* **270,** 12035–12047
16. Hiraoka, N., Petryniak, B., Nakayama, J., Tsuboi, S., Suzuki, M., Yeh, J. C., Izawa, D., Tanaka, T., Miyasaka, M., Lowe, J. B., and Fukuda, M. (1999) *Immunity* **11,** 79–89
17. Fukuda, M., Hiraoka, N., and Yeh, J. C. (1999) *J. Cell Biol.* **147,** 467–470
18. Fukuda, M., Hiraoka, N., Akama, T. O., and Fukuda, M. N. (2001) *J. Biol. Chem.* **276,** 47747–47750
19. Bistrup, A., Bhakta, S., Lee, J. K., Belov, Y. Y., Gunn, M. D., Zuo, F. R., Huang, C. C., Kannagi, R., Rosen, S. D., and Hemmerich, S. (1999) *J. Cell Biol.* **145,** 899–910
20. Yeh, J. C., Hiraoka, N., Petryniak, B., Nakayama, J., Ellies, L. G., Rabuka, D., Hindsgaul, O., Marth, J. D., Lowe, J. B., and Fukuda, M. (2001) *Cell* **105,** 957–969
21. Streeter, P. R., Rouse, B. T., and Butcher, E. C. (1988) *J. Cell Biol.* **107,** 1853–1862
22. Tangemann, K., Bistrup, A., Hemmerich, S., and Rosen, S. D. (1999) *J. Exp. Med.* **190,** 935–942
23. Hemmerich, S., Bistrup, A., Singer, M. S., van Zante, A., Lee, J. K., Tsay, D., Peters, M., Carminati, J. L., Brennan, T. J., Carver-Moore, K., Leviten, M., Fuentes, M. E., Ruddle, N. H., and Rosen, S. D. (2001) *Immunity* **15,** 237–247
24. Bierhuizen, M. F., and Fukuda, M. (1992) *Proc. Natl. Acad. Sci. U. S. A.* **89,** 9326–9330
25. Ellies, L. G., Tsuboi, S., Petryniak, B., Lowe, J. B., Fukuda, M., and Marth, J. D. (1998) *Immunity* **9,** 881–890
26. Maly, P., Thall, A., Petryniak, B., Rogers, C. E., Smith, P. L., Marks, R. M., Kelly, R. J., Gersten, K. M., Cheng, G., Saunders, T. L., Camper, S. A., Camphausen, R. T., Sullivan, F. X., Isogai, Y., Hindsgaul, O., von Andrian, U. H., and Lowe, J. B. (1996) *Cell* **86,** 643–653
27. Bruehl, R. E., Bertozzi, C. R., and Rosen, S. D. (2000) *J. Biol. Chem.* **275,** 32642–32648
28. Bierhuizen, M. F., Maemura, K., and Fukuda, M. (1994) *J. Biol. Chem.* **269,** 4473–4479
29. Hiraoka, N., Nakagawa, H., Ong, E., Akama, T. O., Fukuda, M. N., and Fukuda, M. (2000) *J. Biol. Chem.* **275,** 20188–20196
30. Kytzia, H. J., and Sandhoff, K. (1985) *J. Biol. Chem.* **260,** 7568–7572
31. Homeister, J. W., Thall, A. D., Petryniak, B., Maly, P., Rogers, C. E., Smith, P. L., Kelly, R. J., Gersten, K. M., Askari, S. W., Cheng, G., Smithson, G., Marks, R. M., Misra, A. K., Hindsgaul, O., von Andrian, U. H., and Lowe, J. B. (2001) *Immunity* **15,** 115–126
32. Finger, E. B., Puri, K. D., Alon, R., Lawrence, M. B., von Andrian, U. H., and Springer, T. A. (1996) *Nature* **379,** 266–269
33. Munro, S. (1991) *EMBO J.* **10,** 3577–3588
34. Aoki, D., Lee, N., Yamaguchi, N., Dubois, C., and Fukuda, M. N. (1992) *Proc. Natl. Acad. Sci. U. S. A.* **89,** 4319–4323
35. Arbones, M. L., Ord, D. C., Ley, K., Ratech, H., Maynard-Curry, C., Otten, G., Capon, D. J., and Tedder, T. F. (1994) *Immunity* **1,** 247–260
36. Suzuki, A., Andrew, D. P., Gonzalo, J. A., Fukumoto, M., Spellberg, J., Hashiyama, M., Takimoto, H., Gerwin, N., Webb, I., Molineux, G., Amakawa, R., Tada, Y., Wakeham, A., Brown, J., McNiece, I., Ley, K., Butcher, E. C., Suda, T., Gutierrez-Ramos, J. C., and Mak, T. W. (1996) *Blood* **87,** 3550–3562
37. Satomaa, T., Renkonen, O., Helin, J., Kirveskari, J., Mäkitie, and Renkonen R. (2002) *Blood* **99,** 2609–2611
38. Bargatze, R. F., Jutila, M. A., and Butcher, E. C. (1995) *Immunity* **3,** 99–108
39. Kunkel, E. J., Ramos, C. L., Steeber, D. A., Muller, W., Wagner, N., Tedder, T. F., and Ley, K. (1998) *J. Immunol.* **161,** 2449–2456
40. Kimura, N., Mitsuoka, C., Kanamori, A., Hiraiwa, N., Uchimura, K., Muramatsu, T., Tamatani, T., Kansas, G. S., and Kannagi, R. (1999) *Proc. Natl. Acad. Sci. U. S. A.* **96,** 4530–4535
41. Uchimura, K., El-Fasakhany, F. M., Hori, M., Hemmerich, S., Blink, S. E., Kansas, G. S., Kanamori, A., Kumamoto, K., Kannagi, R., and Muramatsu, T. (2002) *J. Biol. Chem.* **277,** 3979–3984
42. Uchimura, K., Muramatsu, H., Kadomatsu, K., Fan, Q. W., Kurosawa, N., Mitsuoka, C., Kannagi, R., Habuchi, O., and Muramatsu, T. (1998) *J. Biol. Chem.* **273,** 22577–22583
43. Mitoma, J., Petryniak, B., Hiraoka, N., Yeh, J. C., Lowe, J. B., and Fukuda, M. (2003) *J. Biol. Chem.* **278,** 9953–9961
44. Leppänen, A., Yago, T., Votto, V. I., McEver, R. P., and Cummings, R. D. (2003) *J. Biol. Chem.* **278,** 26391–26400
45. Fieger, C. B., Sassetti, C. M., and Rosen, S. D. (2003) *J. Biol. Chem.* **278,** 27390–27398
46. Clark, R. A., Fuhlbrigge, R. C., and Springer, T. A. (1998) *J. Cell Biol.* **140,** 721–731
47. Wang, L., Brown, J. R., Varki, A., and Esko, J. D. (2002) *J. Clin. Invest.* **110,** 127–136
48. Kawashima, H., Watanabe, N., Hirose, M., Sun, X., Atarashi, K., Kimura, T., Shikata, K., Matsuda, M., Ogawa, D., Heljasvaara, R., Rehn, M., Pihlajaniemi, T., and Miyasaka, M. (2003) *J. Biol. Chem.* **278,** 13069–13076
49. Yeh, J. C., Ong, E., and Fukuda, M. (1999) *J. Biol. Chem.* **274,** 3215–3221
50. Shiraishi, N., Natsume, A., Togayachi, A., Endo, T., Akashima, T., Yamada, Y., Imai, N., Nakagawa, S., Koizumi, S., Sekine, S., Narimatsu, H., and Sasaki, K. (2001) *J. Biol. Chem.* **276,** 3498–3507
51. Smith, P. L., Gersten, K. M., Petryniak, B., Kelly, R. J., Rogers, C., Natsuka, Y., Alford, J. A., III, Scheidegger, E. P., Natsuka, S., and Lowe, J. B. (1996) *J. Biol. Chem.* **271,** 8250–8259
52. Ujita, M., McAuliffe, J., Schwientek, T., Almeida, R., Hindsgaul, O., Clausen, H., and Fukuda, M. (1998) *J. Biol. Chem.* **273,** 34843–34849
53. Priatel, J. J., Chui, D., Hiraoka, N., Simmons, C. J., Richardson, K. B., Page, D. M., Fukuda, M., Varki, N. M., and Marth, J. D. (2000) *Immunity* **12,** 273–283

[CANCER RESEARCH 64, 4257–4262, June 15, 2004]

Functional Correlation of Trophinin Expression with the Malignancy of Testicular Germ Cell Tumor

Shingo Hatakeyama,[1] Chikara Ohyama,[1] Shingo Minagawa,[1] Takamitsu Inoue,[1] Hideaki Kakinuma,[1] Atsushi Kyan,[2] Yoichi Arai,[2] Tomoaki Suga,[3] Jun Nakayama,[4] Tetsuro Kato,[1] Tomonori Habuchi,[1] and Michiko N. Fukuda[5]

[1]Department of Urology, Akita University School of Medicine, Akita, Japan; [2]Department of Urology, Tohoku University School of Medicine, Sendai, Japan; [3]Department of Internal Medicine, Shinshu University School of Medicine and [4]Department of Pathology, Shinshu University Graduate School of Medicine, Matsumoto, Japan; and [5]Glycobiology Program, Cancer Research Center, The Burnham Institute, La Jolla, California

ABSTRACT

Trophinin is a membrane protein that is potentially involved in human embryo implantation by mediating homophillic cell adhesion between trophoblastic cells and endometrial cells. Trophinin expression by maternal cells may be induced by the embryo that secretes human chorionic gonadotropin (hCG). Because the process of tumor metastasis resembles that of trophoblast invasion and proliferation during embryo implantation, we hypothesized that testicular cancers that synthesize hCG express trophinin thus becoming aggressive trophoblast-like cells. We screened paraffin-embedded orchiectomy specimens of 158 patients with testicular germ cell tumor by immunohistochemistry using antitrophinin antibody. This screening identified trophinin-positive specimens with the frequencies 39 of 91 (43%) in stage I, 14 of 24 (58%) in stage II, and 41 of 43 (95%) in stage III ($P < 0.001$). Thus, trophinin expression positively correlates with clinical stage. Remarkably, trophinin was found in all of the cases (33 of 33) with lung metastasis. The levels of serum hCG-β were significantly higher in the patients with trophinin-positive tumors than those with trophinin-negative tumors ($P = 0.004$). To determine whether trophinin promotes aggressiveness of the cell, trophinin-negative human seminona cell line JKT-1 was stably transfected with a mammalian expression vector containing trophinin cDNA. *In vitro* assays revealed that trophinin-expressing JKT-1-Tro cells are more invasive than JKT-1-mock cells, whereas there are no differences between JKT-1-Tro and JKT-1-mock in their proliferation activity. Upon orthotopic inoculation to athymic nude mice, JKT-1-Tro cells exhibited i.p. metastases in all of the mice ($n = 5$), whereas JKT-1-mock produced no metastases ($n = 5$). These results suggest strongly that trophinin enhances invasiveness of the cells and promotes metastasis of testicular germ cell tumor.

INTRODUCTION

Testicular germ cell tumor remains the most common solid malignancy in young men between 15 and 35 years of age (1). Recent statistics suggest disturbing trends that incidence of testicular germ cell tumor is increasing, and the age at which testicular germ cell tumor develops is becoming younger (2, 3). With the introduction of *cis*-platinum chemotherapy in the late 1970s, the survival rate of patients with testicular germ cell tumor now exceeds 90% (4, 5). However, it is still difficult to treat advanced testicular germ cell tumor with multiple distant metastases.

In germ cell tumors, all of the patients of choriocarcinoma, 40–60% of embryonal carcinoma, and 5–10% of patients with pure seminoma show the elevation of human chorionic gonadotrophin (hCG) β in their sera (6). The hCG is a 38-kDa glycoprotein, which is composed of α and β polypeptide chains. The hCG is normally produced by trophoblastic cells in the placenta (7). The β subunit of hCG is one of the tumor markers of germ cell tumors, and this value correlates well with the patient populations having clinical stages I, II, and III testicular tumors (6).

Trophinin is a membrane protein that potentially mediates the initial adhesion between human embryo and uterine epithelial cells through a unique apical cell adhesion between two cell types, trophoblastic cells and endometrial epithelial cells (8–10). In humans, endometrium is under strict hormonal control and is generally not permissive to implantation. Trophinin is not expressed during proliferative and ovulation phases, whereas strong expression of trophinin within a restricted area of human endometrium was detected at early secretory phase or time of implantation window (8–10). Recent findings of ectopic pregnancy suggest strongly that trophinin expression by maternal cells is embryo-dependent. Thus, hCG-β secreted from the implanting embryo induces trophinin in maternal cells through jaxtacrine manner (11).

The processes of human embryo implantation, which include rapid proliferation and invasion of trophoblasts, are often compared with the aggressive behaviors of malignant cancer cells (12). Recent studies have suggested that hCG expressed in trophoblast and various malignant tumors promotes cellular motility (6–7). These observations prompted us to investigate the possible role of hCG in testicular germ cell tumors. We describe here the expression of trophinin and hCG-β in testicular germ cell tumors and the effect of ectopic expression of trophinin on cellular motility, proliferation, and metastatic activities.

MATERIALS AND METHODS

Human Testicular Germ Cell Tumor Specimens. Testicular germ cell tumor specimens from 158 patients (76 seminoma and 82 nonseminomatous germ cell tumors) at various clinical stages were collected between 1981 and 2002. Informed consent was obtained from all of the patients whose specimens were used in this study. Pathological findings were recorded according to American Joint Committee on Cancer staging system (13).

Serum hCG-β Measurement. Before orchiectomy, blood sample was obtained by routine venipuncture from each patient and was subjected to serum hCG-β subunit measurement by ELISA.

Immunohistochemistry. Immunohistochemistry for trophinin, tastin, and bystin was performed as described previously (14), except Simple Stain Max PO kit and Simple Stain AEC solution (Nichirei Corp., Tokyo, Japan), according to manufacturer's instructions. Anti-hCG antibody was obtained from Nichirei Corporation.

Cell Line and Cell Culture. JKT-1 is a human testicular seminoma cell line provided by Dr. Keigo Kinugawa (Department of Urology, Kawasaki Medical School, Kurashiki, Japan; Ref. 15). This cell line was maintained in α-MEM containing 10% fetal bovine serum in a humidified 5% CO_2 atmosphere at 37°C.

Establishment of Stable Transfectant. JKT-1 cells, which do not express trophinin, were transfected with pcDNA1-trophinin (8) using LipofectAMINE (Life Technologies, Inc.) as described in the protocol provided by the supplier. After 2 weeks in G418 selection (400 μg/ml; Life Technologies, Inc.), 20 single colonies were examined for immunochemical detection of trophinin using antitrophinin mouse monoclonal antibody and FITC-conjugated goat affinity-purified $F(ab')_2$ fragment specific to mouse IgM (Cappel). Three stable transfectants expressing trophinin were established (JKT-1-Tro). Among

Received 3/1/04; revised 3/29/04; accepted 4/7/04.

Grant support: Grants 15659377 (to C. Ohyama) and B-15390115 (to J. Nakayama) from the Japan Society for the Promotion of Science, a grant from Kyowa Medex (to M. Fukuda), and NIH Grant HD34108 (to M. Fukuda).

The costs of publication of this article were defrayed in part by the payment of page charges. This article must therefore be hereby marked *advertisement* in accordance with 18 U.S.C. Section 1734 solely to indicate this fact.

Requests for reprints: Michiko N. Fukuda, Glycobiology Program, Cancer Research Center, The Burnham Institute, 10901 North Torrey Pines Road, La Jolla, CA 92037. Phone: (858) 646-3143; Fax: (858) 646-3193; E-mail: michiko@burnham.org.

Table 1 *Association of trophinin immunostaining and clinical stage*

Study group	All positive/ total (%)	Seminoma positive/ total (%)	NSGCT[a] positive/ total (%)
Clinical stage			
I + II	39 + 14/91 + 24 (46)	17 + 6/56 + 12 (34)	22 + 8/35 + 12 (64)
III	41/43 (95)	6/8 (75)	28/28 (100)
P	<0.001	<0.05	<0.001
Lung metastasis			
−	61/125 (49)	24/71 (34)	37/54 (69)
+	33/33 (100)	5/5 (100)	28/28 (100)
P	<0.001	<0.05	<0.001

[a] NSGCT, nonseminomatous germ cell tumor.

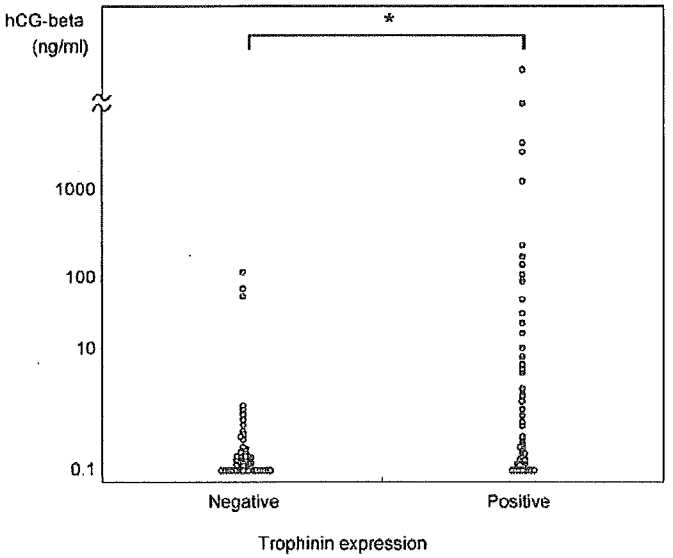

Fig. 1. Correlation between trophinin expression and serum human chorionic gonadotropin (*hCG*)-β concentration. *, statistical significance between trophinin-positive and -negative groups. ($P = 0.004$, Mann-Whitney U test).

the stable transfectants, two clones (JKT-1-Tro-1 and -2) were subjected to tumor assays. As a control cell line, mock-transfectant (vector only) JKT-1-pcDNA1 cells were used.

Flow Cytometric Analysis. JKT-1-Tro cells and mock transfectant cells were assessed by fluorescence-activated cell sorting analysis after incubation with antitrophinin antibody (mouse IgM; Ref. 14) followed by incubation with FITC-conjugated secondary antibodies. Analyses were carried out by FACSort flow cytometry using the CellQuest program (Becton Dickinson).

Growth Rate of Cell Lines. JKT-1-Tro cells and mock-transfectant cells were seeded in 96-well plates at 10^5 cells/ml in α-MEM containing 10% fetal bovine serum and 400 μg/ml of G418 and cultured for various times. The number of living cells was measured each day using the Cell Counting kit (Wako Pure Chemical Industries, Tokyo, Japan). Triplicate cultures were used for each analysis.

Motility and Invasion Assays. A transwell cell culture chamber (Costar, Cambridge, MA) was used for *in vitro* motility and invasion assays with modifications (16). Briefly, the bottom of the upper chamber was sealed with a polyvinylpyrrolidone-free polycarbonate filter with a pore size of 8 nm. The lower face was covered with 50 μg/ml fibronectin (Wako Pure Chemical Industries) in α-MEM medium. Cells (1×10^5) were plated in the upper chamber and incubated in a humidified CO_2 incubator at 37°C for 5 h. The lower chamber was filled with serum-free α-MEM medium. Cells that did not migrate through the membrane were removed, and the cells that migrated to the lower face of the membrane were fixed with methanol followed by Giemsa staining. The number of cells on the lower face was counted under microscope. The mean number of 10 different fields was plotted. For the invasion assay, the upper face of the filter was covered with 100 μg/ml Matrigel (Collaborative Research, Bedford, MA), and the number of cells on the lower face was counted. These assays were carried out in triplicate. The SD of these values was always within 5%.

Orthotopic Tumor Cell Inoculation. BALB/c nude (*nu/nu*) mice, 6–8-week-old males obtained from CLEA Japan, Inc. (Tokyo, Japan), were used for orthotopic tumor cell injection. Mice were anesthetized with avertin, and intratesticular injection was performed. JKT-1-Tro cells (2×10^6) and mock-transfected JKT-1 cells were suspended in 100 μl of serum-free α-MEM and inoculated into the right testis. Three weeks after injection, mice were sacrificed, and testis and other organs having metastasis were removed and fixed with a buffered formalin solution.

Adhesion of JKT-1 Cells to Endothelial Cells. The human pulmonary microvascular endothelial cells (HMVEC-L) were obtained from the Sanko Junyaku Co., Ltd. (Tokyo, Japan) and were cultured in EGM-2M medium containing microvascular endothelial cell growth factors, antimicrobials, and 5% fetal bovine serum to confluence in 24-well culture plate. The wells were washed three times with PBS. JKT-1-Tro cells and JKT-1-mock cells were detached from the plate with trypsin and resuspended in α-MEM (1% fetal bovine serum) and added at 1×10^5 cells/ml on a monolayer of HMVEC-L. For the antibody treatment, JKT-1-Tro cells were incubated with monoclonal antibody against trophinin on ice for 30 min, washed with PBS, and added onto the HMVEC-L monolayer.

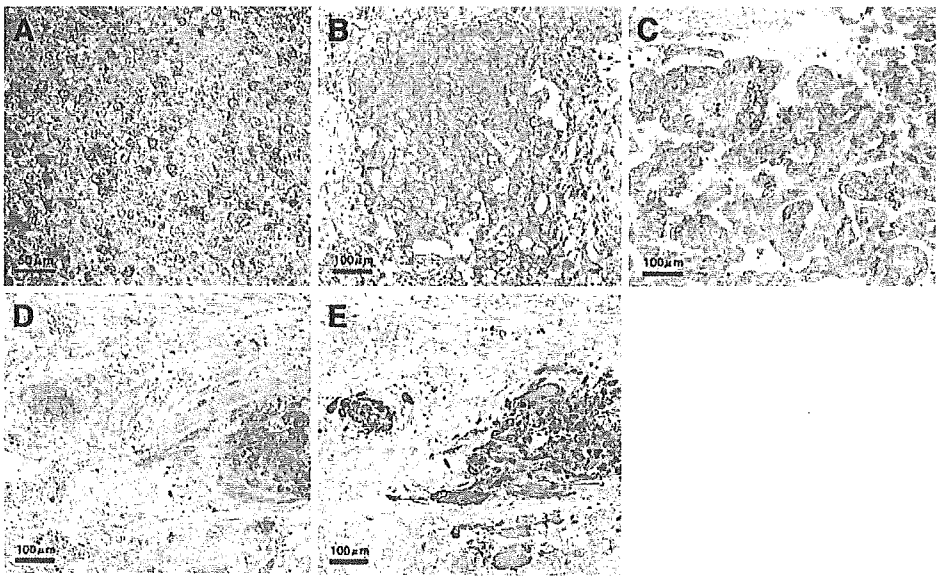

Fig. 2. Immunohistochemistry of human testicular germ cell tumors. Paraffin sections of testicular germ cell tumors were stained with antitrophinin antibody and antihuman chorionic gonadotropin antibody. Each specimen shows seminoma (*A*), embryonal carcinoma (*B*), yolk sac tumor (*C*), and choriocarcinoma (*D–E*). *D* and *E* are serial sections of the same specimen stained with antitrophinin antibody (*D*) and antihuman chorionic gonadotropin antibody (*E*). Counterstaining was performed by hematoxylin.

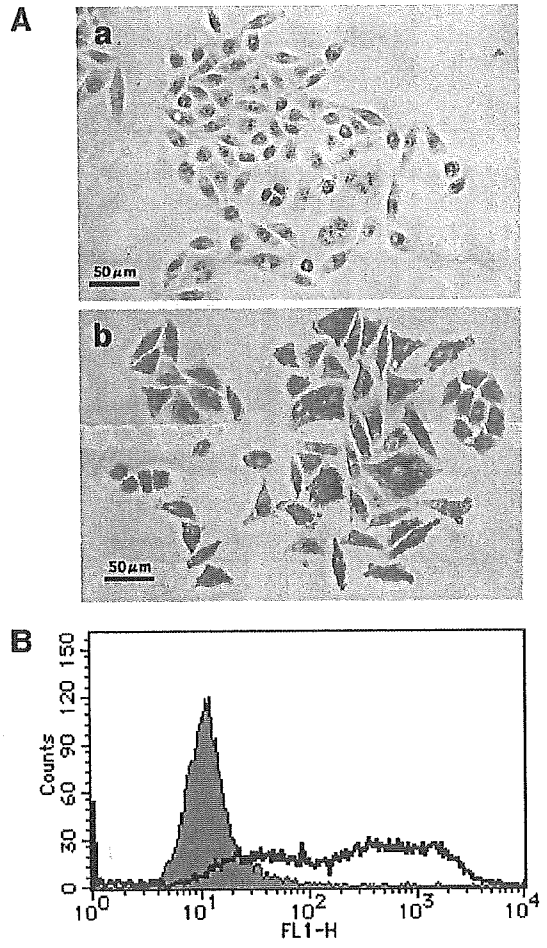

Fig. 3. Expression of trophinin in JKT-1-Tro cells. *A*, fixed but not permeabilized JKT-1 cells were reacted with antitrophinin antibody for detection of trophinin on the cell surface. Note that JKT-1-mock cells (*panel a*) are negative for trophinin, whereas stable transfectant for trophinin, JKT-1-Tro-1 cells (*panel b*) are positively stained with antitrophinin antibody. Another stable transfectant, JKT-1-Tro-2 cells, were also positively stained with antitrophinin antibody with similar intensity (data not shown). *B*, flow cytometry analysis of JKT-1 cells. Cell surface expression of trophinin was confirmed by flow cytometry analysis of intact JKT-1-Tro cells using antitrophinin antibody. JKT-1-Tro-1 cells (*open histogram*) showed higher intensity than mock transfectants (*closed histogram*). JKT-1-Tro-2 cells showed a similar pattern to that of JKT-1-Tro-1 cells (data not shown).

RESULTS

Expression of Trophinin by Patients with Testicular Tumors. Immunohistochemistry of testicular tumors revealed significant positive correlations between trophinin expression and clinical stage (Ref. 17; Table 1). Especially, all of the tumor specimens from patients with lung metastasis were positive for trophinin. Furthermore, serum hCG-β concentration was positively correlated with trophinin expression (Fig. 1), which was confirmed by immunohistochemistry (Fig. 2, *C* and *D*).

We screened 158 patients with testicular tumors. Among them, trophinin was found positive in 39 of 91 (43%) patients in stage I, 14 of 24 (58%) patients in stage II, and 41 of 43 (95%) patients in stage III ($P < 0.001$). Testicular germ cell tumors with stage III were positive strongly for trophinin. Serum hCG concentration was significantly higher in the trophinin-positive group than in the trophinin-negative group (Fig. 1). Remarkably, all of the specimens with lung metastasis were trophinin positive, regardless of seminoma or nonseminomatous germ cell tumor (Table 1). Thus, trophinin expression in the tumor correlates positively with distant metastasis and high levels of serum hCG. These observations suggest that the trophinin-positive testicular tumors are more aggressive than trophinin-negative tumors.

Properties of Trophinin-Positive Seminoma Cell Line, JKT-1-Tro. Because the function of trophinin in cell proliferation and invasion are not known, we investigated whether trophinin plays a role of malignant phenotype in testicular germ cell tumor. Human seminoma cell line JKT-1 does not express trophinin nor trophinin-associated cytoplasmic proteins tastin and bystin (data not shown). JKT-1 cells were transfected with a mammalian expression vector having trophinin cDNA. JKT-1-Tro cells and JKT-1-mock cells obtained by transfection of trophinin cDNA and vector without insert, respectively, were evaluated for their expression of trophinin using antitrophinin antibody by immunocytochemistry (Fig. 3*A*) and flow cytometry (Fig. 3*B*) analysis. Thus, two clones for JKT-1-Tro express trophinin on the

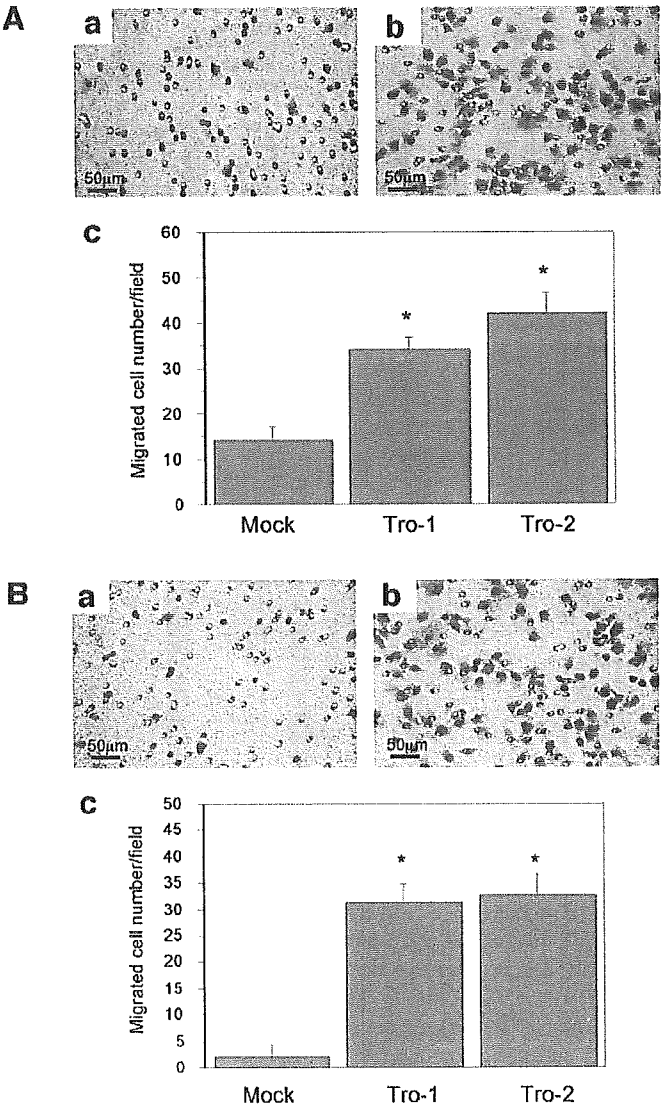

Fig. 4. Motility and invasion activities of JKT-1 cells. Motility and invasion activities of JKT-1 transfectants were assayed by transmigration chambers. *A*, JKT-1-mock cells (*panel a*) and JKT-1-Tro-1 cells (*panel b*) migrated through a filter membrane from uncoated upper chamber to fibronectin coated lower chamber. Cell number count (*panel c*) showed the significant increase of motility of trophinin expressing JKT-1 cells. *, statistical significance against the mock-transfectant cells ($P < 0.001$, Mann-Whitney *U* test). *B*, JKT-1-mock cells (*panel a*) and JKT-1-Tro-1 cells (*panel b*) migrated through Matrigel-coated filter membrane. Invasion potential was significantly increased in JKT-1-Tro cells (*panel c*). *, statistical significance against the mock-transfectant cells ($P < 0.001$, Mann-Whitney *U* test); *bars*, ±SD.

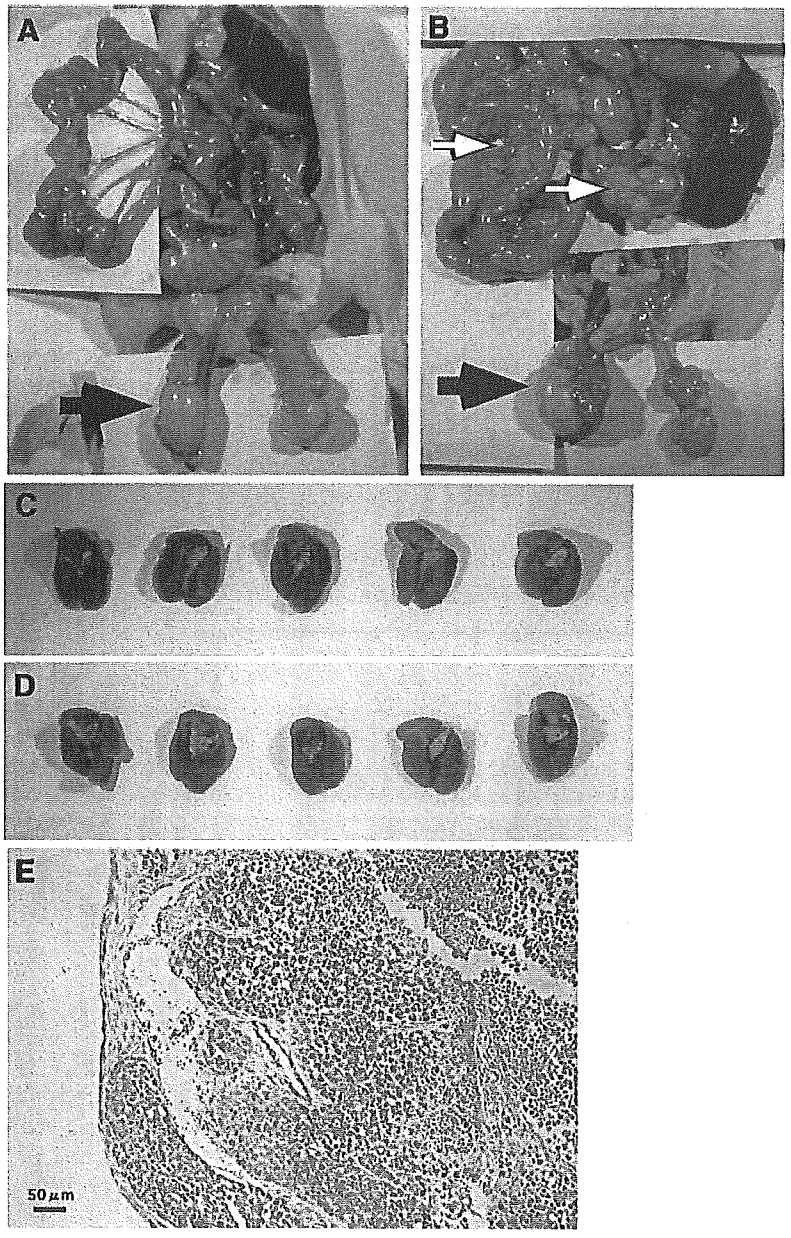

Fig. 5. Tumor formation by JKT-1-Tro cells in the nude mice. JKT-1-mock cells (*A*) and JKT-1-Tro-1 cells (*B*; 2×10^6 cells each) were inoculated in the right testis. JKT-1-Tro-1 cells produced intra-abdominal metastasis in all of the mice ($n = 5$; *B*), whereas JKT-1-mock cells produced no metastasis ($n = 5$; *A*). No differences in the size of testes were seen between JKT-1-mock and JKT-1-Tro (*black arrows*). Note that JKT-1-Tro-1 produces numerous mesenteric metastases (*open arrows in B*). JKT-1 mock (*C*) or JKT-1-Tro-1 (*D*) produced no lung metastasis. JKT-1-Tro-2 cells showed also the same result as JKT-1-Tro-1 (data not shown). *E*, immunohistochemistry of metastasized tumor with antitrophinin antibody.

cell surface, whereas two clones for JKT-1-mock do not (Fig. 3*B*). Thus, clonal variations among JKT-1-Tro and those among JKT-1-mock are considered to be minimum.

Because malignancy is closely associated with cell proliferation activity, we determined cell numbers of JKT-1-Tro cells and JKT-1-mock cells. The results show no significant difference between JKT-1-Tro cells and JKT-1-mock cells in cell numbers during *in vitro* culture (data not shown), suggesting that acquisition of trophinin does not solely enhance cell proliferation activity of JKT-1 cells cultured *in vitro*.

Next, JKT-1-Tro cells and JKT-1-mock cells were subjected to motility and invasion assays using a transwell cell culture system. Fibronectin and Matrigel were coated on the lower and upper face of the transwell for testing motility and invasion, respectively. These assays revealed that JKT-1-Tro cells are significantly mobile (Fig. 4*A*) and invasive (Fig. 4*B*) compared with JKT-1-mock cells. The possibility for clonal deviations of these results is excluded, because the differences between JKT-1-Tro clones were not significant.

Metastatic Potential of JKT-1-Tro Cells *in Vivo* in the Mouse. Because clinical data (Table 1) indicated a strong correlation between trophinin-positive testicular tumors and lung metastasis, we tested whether JKT-1-Tro cells metastasize to the lung in the mouse. JKT-1-Tro cells and JKT-1-mock cells were inoculated in the right testis of the nude mice. Three weeks after inoculation, mice were sacrificed to determine the tumor size and metastasis. JKT-1-Tro cells produced massive intra-abdominal metastasis in all of the mice ($n = 5$), whereas mock transfectants produced no metastasis ($n = 5$; Fig. 5, *A* and *B*). Although the lung metastasis is common in the cancer patients, evidence for the lung metastasis has not been obtained by these experiments (Fig. 5, *C* and *D*). Immunohistochemistry using monoclonal antitrophinin antibody showed that mesenteric metastases produced in the mouse were positive for trophinin (Fig. 5*E*).

Although the experiments using the mice did not show the lung metastasis, the lung metastasis and trophinin expression are hallmark in the testicular cancers in humans (Table 1). To gain insight into the mechanisms for lung metastasis of trophinin-positive testicular germ

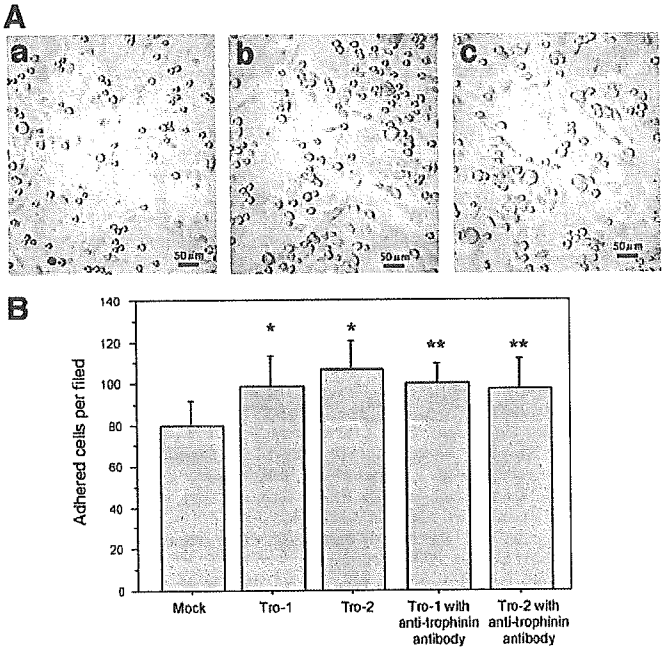

Fig. 6. Adhesion of mock transfectants and JKT-1-Tro cells to human lung microvascular endothelial cells (HMVEC-L). *A*, representative photomicrographs of JKT-1-Tro cells adhered to HMVEC-L. Each shows (*panel a*) mock transfectants adhered to HMVEC-L, (*panel b*) JKT-1-Tro-1 cells adhered to HMVEC-L, and (*panel c*) JKT-1-Tro-1 cells pretreated with antitrophinin antibody and adhered to HMVEC-L. JKT-1-Tro-2 cells showed the same result as JKT-1-Tro-1 (data not shown). *B*, numbers of JKT-1-Tro cells adhered to the HMVEC-L. *, statistical significance between JKT-1-Tro and the mock-transfectant cells ($P < 0.001$, Mann-Whitney U test). Note that there are no effects of antitrophinin antibody on the adhesion of JKT-1-Tro-1 and -2 cells. * *, statistical significance with or without antitrophinin antibody treatment. ($P = 0.3$, Mann-Whitney U test); *bars*, ±SD.

cell tumors, we compared the adhesion of JKT-1-Tro cells and JKT-1-mock cells to human lung microvascular endothelial cells by cell adhesion assay *in vitro*. As shown in Fig. 6, JKT-1-Tro cells were only slightly more adhesive to HMVEC-L than JKT-1-mock cells, whereas antitrophinin antibody had no effect on the adhesion between JKT-1-Tro cells and HMVEC-L (Fig. 6). These results suggest that trophinin is not the factor determining the adhesion of tumor cells to HMVEC-L.

DISCUSSION

Testicular germ cell tumor is one of the few neoplasms associated with accurate serum marker, hCG (6). The hCG is found in the placenta in pregnant women (18) but not in any tissue from healthy men. This allows careful follow-up in men with testicular germ cell tumor early in the course of the disease (19, 20). In germ cell tumors and the placenta, syncytiotrophoblastic cells are responsible for the production of hCG. Although both human and mouse produce testicular germ cell tumors, spontaneous trophoblastic transformation of cancer cells does not naturally occur in the mouse (21). Thus, in humans, trophoblastic transformation occurs in the breast, prostate, bladder, thyroid, colon, lung, and endometrial cancers (22–24).

Studies on embryo implantation have revealed significant differences of this process among mammals (25). Remarkably, ectopic pregnancy occurring at a rate as high as 1.4% in all of the pregnancies in humans (26, 27) does not occur naturally or experimentally in other animals, including nonhuman primates (28–30). As described below, trophoblastic transformation of tumors in humans may be explained by the uniqueness of the β subunit of hCG (11, 31).

The hCG is a 38-kDa glycoprotein hormone composed of α and β polypeptide chains (7). The hCG and its pituitary counterpart, lutropin, comprise a family of heterodimeric glycoprotein hormones, including follitropin and thyrotropin, that share a common α subunit but differ in their hormone-specific β subunit (7). The gene encoding CG-α is homologous to those encoding thyroid-stimulating hormones, of which the structures are evolutionally conserved among wide variety of animals (32). By contrast, CG-β subunit is specific to primates, and human CG-β gene is diverged from the CG-β genes of nonhuman primates (31).

Trophinin mediates homophilic cell adhesion between human trophoblastic cells and endometrial epithelial cells at their respective apical cell surfaces (8, 9). Strong expression of trophinin was found at the human embryo implantation site (14). Trophinin is also expressed during ectopic pregnancies (11). Interestingly, trophinin expression by the fallopian tubal epithelia depends on the existence of implanting embryo. Thus, the maternal epithelia adjacent to the implantation site express trophinin strongly, whereas the maternal cells a few millimeters away from the implantation site barely express trophinin (11). Such spatially restricted trophinin expression suggests the existence of an embryo-derived factor that stimulates the maternal cells for trophinin expression. This embryonic factor may be CG-β, which is secreted from the trophectoderm of the blastocyst (33–35), because the fallopian tubal explants incubated with hCG showed the elevation of trophinin transcripts (11).

In this study, we found that testicular germ cell tumors often express trophinin (Table 1; Figs. 1 and 2). It is noteworthy that trophinin expression positively correlates with the malignancy of testicular tumor, particularly with the metastasis (Table 1). Our data also showed positive correlation between trophinin expression and hCG-β in the sera of the patients (Table 1; Fig. 1). Taken together, hCG-β expressed by human cancer cells might act on the cancer cells in an autocrine manner to induce trophinin expression.

In this study, we showed that ectopic expression of trophinin in JKT-1 cells enhances motility and invasiveness of the cells *in vitro* (Fig. 4). When JKT-1-Tro cells were inoculated into the mouse, they showed massive peritoneal metastasis (Fig. 5). Clinical data of the testicular germ cell tumors (Table 1) showed that testicular germ cell tumors metastasize to the lung (36). This suggested a possibility that trophinin enhances the lung metastasis. However, our experiments using JKT-1-Tro cells did not show the lung metastasis in the mouse (Fig. 5). Such an apparent discrepancy between the mouse experiments and clinical observations may be explained by the expression of tastin and bystin in the lung metastasized tumors (data not shown). The mechanism underlying the lung metastasis of these tumors remains to be defined in the future study.

Because we identified trophinin, tastin, and bystin as proteins with potential involvement in embryo implantation (8–10), functions of these proteins other than cell adhesion has not been described. Because trophinin, tastin, and bystin are expressed in the human placenta during the periods of early stage of placental development (14), it is possible that these proteins are involved in the subsequent trophoblast invasion process triggered by the initial cell adhesion. Therefore, present study is the first to provide with a suggestion that trophinin plays a role in invasion. Future studies should define the mechanisms of how trophinin promotes cellular motility in embryo implantation and cancer metastasis. The information obtained by such studies will help in designing a therapy against trophoblastic neoplasm, including testicular germ cell tumor.

ACKNOWLEDGMENTS

We thank Dr. Elise Lamar for editing the manuscript and Aleli Morse for her secretarial assistance.

REFERENCES

1. Richie JP. Neoplasms of the testis. In: Walsh PC, Retik AB, Vaughan ED, Wein AJ, editors. Campbell's urology. Vol 3. Philadelphia: WB Saunders; p. 2411–52.
2. Huyghe E, Matsuda T, Thonneau P. Increasing incidence of testicular cancer worldwide: a review. J Urol 2003;170:5–11.
3. Merguerian PA. Pediatric genitourinary tumors. Curr Opin Oncol 2003;15:222–6.
4. Gholam D, Fizazi K, Terrier-Lacombe MJ, et al. Advanced seminoma–treatment results and prognostic factors for survival after first-line, cisplatin-based chemotherapy and for patients with recurrent disease: a single-institution experience in 145 patients. Cancer (Phila) 2003;98:745–52.
5. Christian JA, Huddart RA, Norman A, et al. Intensive induction chemotherapy with CBOP/BEP in patients with poor prognosis germ cell tumors. J Clin Oncol 2003;21: 871–7.
6. Madersbacher S, Gerth R, Mann K, Dirnhofer S, Berger P. Gonadotrophin secretion patterns in testicular cancer patients with greatly increased human chorionic gonadotrophin serum concentrations. J Endocrinol 1998;159:451–8.
7. Pierce J, Parsons TF. Glycoprotein hormones: structure and Function. Annu Rev Biochem 1981;50:465–95.
8. Fukuda MN, Sato T, Nakayama J, et al. Trophinin and tastin, a novel cell adhesion complex with potential involvement in embryo implantation. Genes Dev 1995;9: 1199–210.
9. Suzuki N, Zara J, Sato T, et al. A novel cytoplasmic protein, bystin, interacts with trophinin, tastin, and cytokeratin, and may be involved in trophinin mediated cell adhesion between trophoblast and endometrial epithelial cells. Proc Natl Acad Sci USA 1998;95:5027–32.
10. Fukuda MN, Nozawa S. Trophinin, tastin, and bystin: a complex mediating unique attachment between trophoblastic and endometrial epithelial cells at their respective apical cell membranes. Semin Reprod Endocrinol 1999;17:229–34.
11. Nakayama J, Aoki D, Suga T, et al. Implantation-dependent expression of trophinin by maternal fallopian tube epithelia during tubal pregnancies: possible role of human chorionic gonadotrophin on ectopic pregnancy. Am J Pathol 2003;163:2211–9.
12. Denker H-W. Trophoblast-endometrial interactions at embryo implantation: a cell biological paradox. In: Denker H-W, Aplin JD, editors. Trophoblast research. New York: Plenum Medical Book Company; 1990. p. 3–20.
13. Greene FL, Page DL, Fleming ID, et al., editors. AJCC cancer staging manual. Edition 6. New York: Springer-Verlag; 2002. p. 317–22.
14. Suzuki N, Nakayama J, Shih I-M, et al. Expression of trophinin, tastin, and bystin by trophoblast and endometrial cells in human placenta. Biol Reprod 1999;60:621–7.
15. Kinugawa K, Hyodo F, Matsuki T, et al. Establishment and characterization of a new human testicular seminoma cell line, JKT-1. Int J Urol 1998;5:282–7.
16. Albini A, Iwamoto Y, Kleiman HK, et al. A rapid in vitro assay for quntitating the invasive potential of tumor cells. Cancer Res 1987;47:3239–45.
17. Sobin LH, Fleming ID. TNM classification of malignant tumors. Edition 5. Union Internationale Contre le Cancer and the American Joint Committee on Cancer. Cancer (Phila) 1997;80:1803–4.
18. Wilcox AJ, Baird DD, Weinberg CR. The time of implantation of the conceptus and loss of pregnancy. N Engl J Med 1999;340:1796–9.
19. Mazumdar M, Bajorin DF, Bacik J, et al. Predicting outcome to chemotherapy in patients with germ cell tumors: the value of the rate of decline of human chorionic gonadotrophin and alpha-fetoprotein during therapy. J Clin Oncol 2001;19:2534–41.
20. Bellet D, Bidart JM, Jolivet M. A monoclonal antibody against a synthetic peptide is specific for the free native human chorionic gonadotropin beta-subunit. Endocrinology 1984;115:330–6.
21. Tanaka S, Kunath T, Hadjantonakis AK, Nagy A, Rossant J. Promotion of trophoblast stem cell proliferation by FGF4. Science (Wash DC) 1998;282:2072–5.
22. Lehtovirta P, Alfthan H, Vaetiainen J, Stenman U. Skin metastases of gynecological adenocarcinomas affect serum levels of hCG beta but not those of SCC antigen. Tumor Biol 1999;20:251–5.
23. Konishi I, Kuroda H, Mandai M. Gonadotropins and development of ovarian cancer. Oncology 1999;57:45–8.
24. Bellet D, Lazar V, Bieche I, et al. Malignant transformation of nontrophoblastic cells is associated with the expression of chorionic gonadotropin beta genes normally transcribed in trophoblastic cells. Cancer Res 1997;57:516–23.
25. Carson DD, Bagchi I, Dey SK, et al. Embryo implantation. Dev Biol 2000;223:217–37.
26. Brenner PF, Roy S, Mishell DR Jr. Ectopic pregnancy. A study of 300 consecutive surgically treated cases. J Am Med Assoc 1980;243:673–6.
27. Graczykowski JW, Mishell DRJ. Ectopic pregnancy. In: Lobo RA, Mishell DRJ, Paulson RJ, Shoupe D, editors. Mishell's textbook of infertility, contraception, and reproductive endocrinology. Massachusetts: Blackwell Science; 1997. p. 623–37.
28. Orsini MW, McLaren A. Loss of the zona pellucida in mice, and the effect of tubal ligation and ovariectomy. J Reprod Fertil 1967;13:485–99.
29. Tutton DA, Curr DH. The fate of trophoblast within the oviduct in the mouse. Gynecol Obstet Investig 1984;17:18–24.
30. Pauerstein CJ, Eddy CA, Koong MK, Moore GD. Rabbit endosalpinx suppress ectopic implantation. Fertil Steril 1990;54:522–6.
31. Talmadge K, Vamvakopouics WC, Fiddes JC. Evolution of the genes for the subunits of human chorionic gonadotropin and luteinizing hormone. Nature (Lond) 1984;307: 37–40.
32. Li MD, Ford JI. A comprehensive evolutionary analysis based on nucleotide and amino acid sequences of the a- and b-subunits of glycoprotein hormone gene family. J Endocrinol 1998;156:529–42.
33. Jurisicova A, Antenos M, Kapasi K, Meriano J, Casper RF. Ability in the expression of trophectodermal markers b-human chorionic gonadotrophin, human leukocyte antigen-G and pregnancy specific b-1 glycoprotein by the human blastocyst. Human Reprod 1999;14:1852–8.
34. Lopata A, Oliva K, Stanton PG, Robertson DM. Analysis of chorionic gonadotrophin secreted by cultured human blastocysts. Mol Hum Reprod 1997;3:517–21.
35. Licht P, Russu V, Wildt L. On the role of human chorionic gonadotropin (hCG) in the embryo-endometrial microenvironment: implications for differentiation and implantation. Semin Reprod Med 2001;19:37–47.
36. Suita S, Shono K, Tajiri T, et al. Malignant germ cell tumors: clinical characteristics, treatment, and outcome. A report from the study group for Pediatric Solid Malignant Tumors in the Kyushu Area, Japan. J Pediatr Surg 2002;37:1703–6.

DOI 10.1002/pmic.200401286 *Proteomics* 2005, *5*, 4274–4286

REGULAR ARTICLE

Protein expression pattern distinguishes different lymphoid neoplasms

Kazuyasu Fujii[1, 2], Tadashi Kondo[1], Hideki Yokoo[1], Tesshi Yamada[1], Yoshihiro Matsuno[3], Keiji Iwatsuki[2] and Setsuo Hirohashi[1]

[1] Cancer Proteomics Project, National Cancer Center Research Institute, Tokyo, Japan
[2] Department of Dermatology, Okayama University Graduate School of Medicine and Dentistry, Okayama, Japan
[3] Pathology Division, National Cancer Center Research Institute, Tokyo, Japan

To identify proteins associated with the histological subtypes of lymphoid neoplasms, we studied the proteomes of 42 cell lines from human lymphoid neoplasms including Hodgkin's lymphoma (HL; four cell lines), B cell malignancies (19 cell lines), T cell malignancies (16 cell lines), and natural killer (NK) cell lymphoma (three cell lines). The protein spots were sequentially selected by (i) Wilcoxon or Kruskal–Wallis tests to find the spots whose intensity was significantly ($p < 0.05$) different among the cell line groups, (ii) by statistical-learning methods to prioritize the spots according to their contribution to the classification, and (iii) by unsupervised classification methods to validate the classification robustness by the selected spots. The selected spots discriminated (i) between HL cells and other cells, (ii) between the cells from B cell malignancies, T cell malignancies, and NK cell lymphoma cells, and (iii) between HL cells and anaplastic large cell lymphoma cells. Among the 31 informative protein spots, MS identified 24 proteins corresponding to 23 spots. Previous reports did not correlate these proteins to lymphocyte differentiation, suggesting that a proteomic study would identify the novel mechanisms responsible for the histogenesis of lymphoid neoplasms. These proteins may have potential as differential diagnostic markers for lymphoid neoplasms.

Received: May 9, 2004
Revised: February 9, 2005
Accepted: February 11, 2005

Keywords:
2D-DIGE / Lymphoid neoplasm / Multivariate analysis / Statistical-learning method

1 Introduction

The recent development of proteomic technologies allows us to describe more than 1000 features of protein expression in a quantitative and reproducible way. The proteomic approach has been used to address many biological questions, and has wide practical utility in the field of medicine [1]. Because the final outcome of genetic and epigenetic events is the content of proteins in the cell, proteomics is conceptually the best and the most accurate and valuable modality for studying the mechanisms of biological phenotypes. In the post-genome era, genome databases coupled with modern high-throughput screening systems, including DNA microarrays and SAGE, have enabled a comprehensive understanding of mRNA expression [2]. However, many lines of evidence suggest that mRNA expression reflects protein expression for only a small proportion of genes [3–6]. Further, PTMs such as phosphorylation and glycation cannot be predicted by measuring the amount of mRNA or by studying nucleic acid sequences. These difficulties underline the potential advantages of proteomic over transcriptomic approaches. However, comprehensive profiling of all proteins expressed in cells has not yet been achieved, and proteomic technologies equivalent to DNA microarray and SAGE are not presently available. For example, many key proteins present in low amounts, such as kinases and oncogene products, are difficult to observe by

Correspondence: Dr. Tadashi Kondo, Cancer Proteomics Project, National Cancer Center Research Institute, 5-1-1 Tsukiji, Chuo-ku, Tokyo 104-0045, Japan
E-mail: takondo@gan2.res.ncc.go.jp
Fax: +81-3-3547-5298

Abbreviations: ALCL, anaplastic large cell lymphoma; **HL**, Hodgkin's lymphoma; **NK**, natural killer

conventional 2-D PAGE. Antibody array may facilitate expression studies, but its utility is limited by the availability of antibodies suitable for the experiments. Therefore, intense efforts are now underway to develop proteomic technologies able to reveal a greater fraction of the proteome, both by modifying present protocols and by developing novel approaches [7–9]. Moreover, as is the case for transcriptomic studies, data-mining techniques, including multivariate analysis and statistical-learning methods, have been used to analyze proteomic data from malignant tumors to find the proteins and the protein networks responsible for the clinicopathological features of cancer [10]. Such use of proteomics will be expanded by the development of new methods.

The differential diagnosis of many lymphoma types has been achieved by morphological findings and immunophenotyping assisted by karyotyping or molecular analysis of specific gene rearrangements [11–14]. However, the subtypes of some lymphomas resemble more than one disease entity [15], and biomarkers for better differential diagnosis have been developed using DNA microarray technologies [16]. Although such studies have successfully identified candidate gene sets, we are still far from a complete description of the biology of lymphoma and therefore other approaches are needed to overcome some of the limitations of present studies.

Here, to demonstrate the utility of the proteomic approach in identifying tumor-specific markers, we used 2-D DIGE and multivariate methods to study a series of lymphoma cell lines. 2-D DIGE captured 83 977 features of the proteome across 42 cell lines from lymphoid neoplasms. This is the first systematic large-scale proteomic study to identify proteins associated with lymphoid neoplasms. Statistical-learning methods were used to distinguish a small number of candidate protein spots specific for the original histology, and subsequent MS study identified the proteins corresponding to the spots.

2 Materials and methods

2.1 Cell lines and protein extraction

The cell lines from human lymphoid neoplasms and their characteristics are summarized in Table 1 [17–55]. They were maintained until use with the culture medium recommended by the distributors. For protein extraction, the cells (5×10^7–1×10^8) were pelleted by centrifugation at 3000 rpm for 5 min and washed three times with PBS. The cells were treated with 10% TCA for 30 min, and then resuspended in urea lysis buffer containing 7 M urea, 2 M thiourea, 3% CHAPS, 1% Triton X-100 for 30 min (1 mL of urea lysis buffer per 100 mg wet weight cells). The cell lysate was centrifuged at 15 000 rpm for 30 min and the supernatant (cellular protein fraction) was recovered. The protein concentration was measured with a Protein Assay Kit (Bio-Rad) and adjusted to 1 mg/mL with urea lysis buffer. All procedures were performed on ice.

2.2 Fluorescence labeling and sample preparation for 2-D DIGE

First, portions of the protein samples from all cell lines were mixed to generate a reference sample. Protein samples from each cell line and the reference sample were then labeled with Cy5 and Cy3, respectively. In brief, the protein sample was adjusted to pH 8.5 with 30 mM Tris. Then, the samples were mixed with 200 pmol of fluorescent dye for 30 min. The labeling reaction was terminated by incubation with 10 mM lysine for 10 min. Urea lysis buffer containing 130 mM DTT and 2% ampholyte was added and incubated for 15 min. Equal amounts of Cy3- and Cy5-labeled protein samples were mixed, and the total volume was adjusted to 1680 μL with urea lysis buffer containing 65 mM DTT and 1% ampholyte. The labeled protein sample was applied to four separate 2-D PAGE gels. All labeling procedures were performed on ice and in the dark.

2.3 2-D PAGE

Proteins were separated by IEF and subsequently by SDS-PAGE, according to our previous report [56]. IEF was performed using linear IPGs (Immobiline Dry Strip, length 24 cm, p*I* range between 4.0 and 7.0; Amersham Biosciences). The IPGs were rehydrated with 420 μL of protein sample at 20°C for 12 h. Proteins were separated on the basis of the p*I* with a total of 96 kVh on an IPGphor (Amersham Biosciences). The IPGs were equilibrated for 20 min in equilibration buffer containing 3 M urea, 50 mM Tris (pH 8.8), 30% glycerol, 1.0% SDS, and 16 mM DTT, and then for 20 min in the same buffer containing 122 mM iodoacetamide instead of DTT. After equilibration, the IPGs were placed on 9–15% gradient polyacrylamide gels and the proteins were separated at 20°C for 15 h at a constant wattage of 17 W per 12 gels. All electrophoresis procedures were performed in the dark.

2.4 Image analysis

After the second-dimension electrophoresis, the gel was scanned at appropriate wavelengths for Cy3 and Cy5 with a MasterImager 2640 (Amersham Biosciences). A pair of Cy3 and Cy5 images was stored as a single apf file and transformed to a pair of tiff files. The relative spot intensity was calculated as the ratio between the absolute intensity of an individual spot and the total intensity of the gel. The relative spot intensity of the Cy5 image was normalized by that of the Cy3 image obtained from the same gel. Since the Cy3 image was generated from the reference sample, a common mixture of all cell lines, this normalization procedure compensates for gel-to-gel variations. Each sample was run on four gels, and average spot intensities were calculated for quantitative comparison.

